

RESEARCH

Open Access



# Dual RNA-seq reveals distinct families of co-regulated and structurally conserved effectors in *Botrytis cinerea* infection of *Arabidopsis thaliana*

Jinfeng Wei<sup>1,2</sup>, Qian Zhou<sup>1,2</sup>, Jing Zhang<sup>1,2</sup>, Mingde Wu<sup>1,2</sup>, Guoqing Li<sup>1,2</sup> and Long Yang<sup>1,2\*</sup>

## Abstract

**Background** *Botrytis cinerea* is a broad-host-range pathogen causing gray mold disease and significant yield losses of numerous crops. However, the mechanisms underlying its rapid invasion and efficient killing of plant cells remain unclear.

**Results** In this study, we elucidated the dynamics of *B. cinerea* infection in *Arabidopsis thaliana* by live cell imaging and dual RNA sequencing. We found extensive transcriptional reprogramming events in both the pathogen and the host, which involved metabolic pathways, signaling cascades, and transcriptional regulation. For the pathogen, we identified 591 candidate effector proteins (CEPs) and comprehensively analyzed their co-expression, sequence similarity, and structural conservation. The results revealed temporal co-regulation patterns of these CEPs, indicating coordinated deployment of effectors during *B. cinerea* infection. Through functional screening of 48 selected CEPs in *Nicotiana benthamiana*, we identified 11 cell death-inducing proteins (CDIPs) in *B. cinerea*.

**Conclusions** The findings provide important insights into the transcriptional dynamics and effector biology driving *B. cinerea* pathogenesis. The rapid infection of this pathogen involves the temporal co-regulation of CEPs and the prominent role of CDIPs in host cell death. This work highlights significant changes in gene expression associated with gray mold disease, underscoring the importance of a diverse repertoire of effectors crucial for successful infection.

**Keywords** *B. cinerea*, Dual RNA-seq, Effector, Co-expression, Plant immunity, Structural conservation, CDIPs

## Background

*Botrytis cinerea* is a devastating plant pathogen that causes gray mold disease in a broad range of hosts. The disease affects over 200 plant species, including some

economically important crops such as grapes, strawberries, and tomatoes [1]. *B. cinerea* can cause substantial pre- and post-harvest losses, making it a major concern for global agriculture [2]. More worrisomely, its spores can be dispersed by wind and rain, resulting in the efficient rapid spread of the disease and making its control highly challenging [3].

Upon infection on plants, *B. cinerea* undergoes a series of complex morphogenetic transitions, including cellular differentiation to form appressoria or infection cushions on the leaf surface, followed by penetration and rapid killing of plant cells [4]. While massive secretion of plant

\*Correspondence:

Long Yang

yanglong@mail.hzau.edu.cn

<sup>1</sup> State Key Laboratory of Agricultural Microbiology, Huazhong Agricultural University, Wuhan, China

<sup>2</sup> Hubei Key Laboratory of Plant Pathology, College of Plant Science and Technology, Huazhong Agricultural University, Wuhan, China



© The Author(s) 2024. **Open Access** This article is licensed under a Creative Commons Attribution-NonCommercial-NoDerivatives 4.0 International License, which permits any non-commercial use, sharing, distribution and reproduction in any medium or format, as long as you give appropriate credit to the original author(s) and the source, provide a link to the Creative Commons licence, and indicate if you modified the licensed material. You do not have permission under this licence to share adapted material derived from this article or parts of it. The images or other third party material in this article are included in the article's Creative Commons licence, unless indicated otherwise in a credit line to the material. If material is not included in the article's Creative Commons licence and your intended use is not permitted by statutory regulation or exceeds the permitted use, you will need to obtain permission directly from the copyright holder. To view a copy of this licence, visit <http://creativecommons.org/licenses/by-nc-nd/4.0/>.

cell wall degrading enzymes (PCWDEs) and non-selective toxins has been recognized as the primary driver of infection [3, 5], recent research has suggested that there may be a more sophisticated infection strategy of *B. cinerea*, including a diverse array of virulence factors employed by the pathogen. This evolving understanding, though incomplete, indicates a multi-layered infection process involving complex interplays of various factors that collectively determine the disease development and severity [6].

Although significant progress has been achieved in characterizing the molecular basis of *B. cinerea* pathogenicity, there are still considerable knowledge gaps. Targeted gene deletion or gene silencing studies have functionally characterized 571 *B. cinerea* genes, these genes represent less than 5% of the fungal genome [6, 7]. These studies focused on various aspects of *B. cinerea* biology, including growth, development, and infection structure formation. However, some fundamental questions remain to be answered, such as how *B. cinerea* overcomes host defenses and achieves rapid tissue invasion and what are the regulatory mechanisms underlying these processes.

Programmed cell death (PCD), including autophagy and apoptosis, is crucial for the interaction between *B. cinerea* and its hosts [8]. Javier Veloso et al. proposed that these pathways differentially regulate host resistance to *B. cinerea* [9]. During the early stages of infection (8–16 hpi), *B. cinerea* suppresses autophagic cell death, allowing it to colonize the host and establish a biotrophic phase. Subsequently (after 16 hpi), *B. cinerea* induces apoptotic cell death, facilitating its transition into the necrotrophic phase. Building upon this framework, we aim to identify key CEPs in *B. cinerea* that modulate PCD.

Effectors are secreted molecules deployed by pathogens to manipulate host physiology and facilitate infection. This diverse arsenal includes PCWDEs, toxins, small RNAs (sRNAs), and various proteins, some of which function as cell death-inducing proteins (CDIPs) or suppressors of plant defenses [4]. *B. cinerea*, a necrotrophic pathogen, has not been reported to possess avirulence (AVR) genes. Therefore, plants usually have no single-gene resistance to *B. cinerea* and no effector-triggered immunity (ETI) response, and their quantitative resistance exclusively relies on pathogen-associated molecular patterns (PAMPs)-triggered immunity (PTI). Common PAMPs recognized by plant receptor-like kinases (RLKs) mainly include chitin and CDIPs [5, 10]. To date, 17 CDIPs have been identified in *B. cinerea*, most of which promote fungal infection by inducing host cell death. BcPG1, an endopolygalacturonase 1 from *B. cinerea*, is a well-characterized CDIP, which is recognized by the receptor-like kinase SIFERL in tomato and thereby

triggers downstream signaling involving SLMAP3K18, SLMAP2K2, and SLMAP2K4, and ultimately induces PCD [11, 12].

Suppressors have been widely reported in biotrophic and hemibiotrophic pathogens and play critical roles in counteracting host defense responses, such as in *Phytophthora infestans* [13] and *Magnaporthe oryzae* [14]. *B. cinerea*, which is similar to *Sclerotinia sclerotiorum*, may exhibit a transient biotrophic phase [15], suggesting the potential presence of effectors with similar suppressive functions in *B. cinerea*. Furthermore, sRNAs acting as effectors in *B. cinerea* function like “cluster bombs,” indiscriminately targeting and silencing host plant transcripts, particularly those involved in immunity [16]. Whether other *B. cinerea* effector proteins exhibit similar disruptive capabilities remains uncertain. Therefore, clarifying the effectors that inhibit plant defense responses or induce PCD is crucial for unraveling the intricate pathogenesis of *B. cinerea*.

The study of plant pathogens is being revolutionized by an ever-increasing number of techniques. Dual RNA-seq has been demonstrated as a powerful technique to reveal the intricate regulatory interplay between hosts and pathogens. It has been employed to dissect the transcriptional dynamics of interactions in various model systems, including *M. oryzae* and rice [17], *Ustilago maydis* and maize [18], *Leptosphaeria maculans* and oilseed rape [19], and *Phytophthora palmivora* and tobacco [20]. There has been one dual RNA-seq study of the necrotrophic fungus *B. cinerea*, which explored early-stage *B. cinerea* infection in strawberry [21]. However, there is still a lack of comprehensive analysis on the entire infection process. Moreover, the rapid advance of artificial intelligence (AI) has revolutionized the prediction of protein structure. AI has been employed to analyze the structural conservation of effector proteins in plant pathogens [22], including the rice blast fungus *M. oryzae* [17, 23] and the apple black spot fungus *Venturia inaequalis* [24]. These technological advances have paved new avenues for investigating the conservation of effector proteins in *B. cinerea*.

In this study, we comprehensively analyzed the morphological and transcriptional reprogramming events occurring throughout the entire infection process (from conidial to aerial hyphae production) of *B. cinerea* on *A. thaliana* through live cell imaging and transcriptomics. Subsequently, we employed bioinformatic approaches to investigate the co-expression, conservation of sequences, and structures among candidate effector proteins (CEPs) in *B. cinerea*. With this information, we then transiently expressed some selected CEPs in *N. benthamiana* to identify CDIPs and cell-death suppressors. Collectively, this study furthers our understanding of the dynamic

interactions between *B. cinerea* and *A. thaliana* and provides valuable insights into the functional roles of *B. cinerea* CEPs during plant–pathogen interactions.

## Results

### Temporal dynamics of *B. cinerea* infection in *A. thaliana*

To elucidate the pathogenesis of *B. cinerea* infection, we investigated the temporal progression of *B. cinerea* conidial invasion into *A. thaliana* leaves at both macroscopic (Fig. 1A) and microscopic (Fig. 1B) levels. Four-week-old *A. thaliana* plants were spray-inoculated with *B. cinerea* conidia at a concentration of  $1 \times 10^5$  conidia/mL. The infection progression was monitored at seven time points of disease development, including 0 (uninfected), 6, 12, 24, 48, 72, and 96 h post-infection (hpi). Fungal invasion was visualized using confocal microscopy after staining with wheat germ agglutinin conjugated with Alexa Fluor 488 (WGA-AF488). According to the observation, the infection process of *B. cinerea* on *A. thaliana* could be summarized into the following key stages (Fig. 1C):

**Attachment and germination (0–12 hpi):** Within the first 6 h of contact with the plant surface, *B. cinerea* conidia started to germinate, forming germ tubes that develop bulbous structures at their tips known as appressoria. By 12 hpi, these germ tubes were elongated and branched, resulting in the formation of numerous appressoria on plant surface, securing the fungus and preparing for invasion (Fig. 1B).

**Invasion and colonization (12–48 hpi):** the appressoria began to form invasive hyphae at 12 hpi, giving rise to invasive hyphae at 24 hpi. These hyphae proliferated and rapidly expanded within the plant tissue till 48 hpi, establishing infection within the host (Fig. 1B).

**Expansion and reproduction (48–96 hpi):** during 48–96 hpi, the fungal mycelia were further developed, forming aerial hyphae and preparing to produce conidia (Fig. 1B), which marks the transition to the next disease cycle, where the fungi prepare to spread and infect new host tissues.

Our observations are consistent with the findings of Bi et al. [4], which demonstrated that the selected time

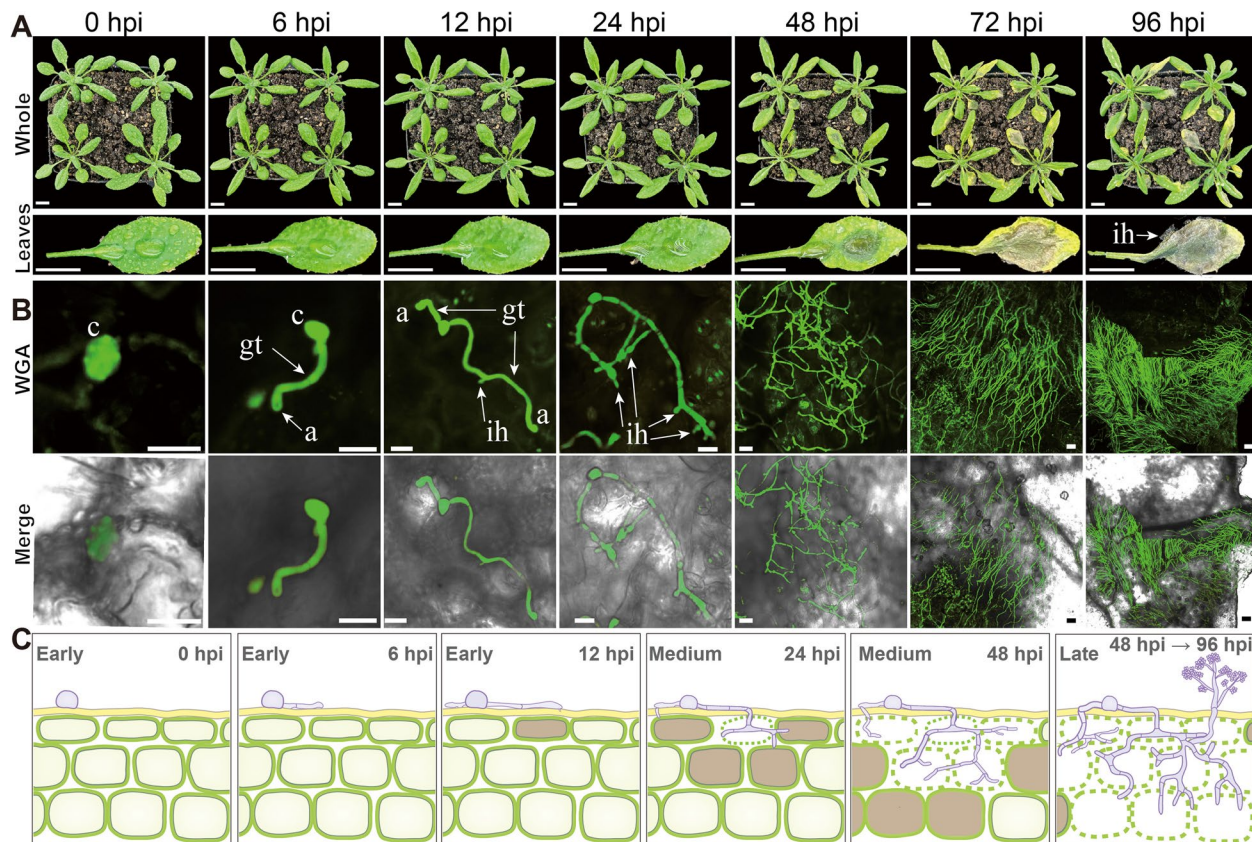


**Fig. 1** Progression of *B. cinerea* infection in *A. thaliana*. **A** Representative images of infected *A. thaliana* leaves at 0, 6, 12, 24, 48, 72, and 96 h post inoculation (hpi). Scale bars = 1 cm. **B** Micrographs depicting the progression of *B. cinerea* B05.10 infection in *A. thaliana* leaves. WGA-AF488 was used to stain fungal hyphae. Scale bars = 20 µm. c conidium, gt germ tube, ih invasive hyphae, ah aerial hyphse. **C** Model depicting stages of *B. cinerea* development on plant leaves corresponding to the time points analyzed by RNA-seq

points could effectively capture the crucial stages of *B. cinerea* invasion, including appressoria formation, appressorial penetration, differentiation of radiating hyphae, and eventual sporulation.

#### Dual transcriptome analysis of *B. cinerea* infection in *A. thaliana*

To elucidate how *B. cinerea* transcriptional reprogramming during infection of *A. thaliana*, we performed dual RNA-seq analysis. Illumina sequencing was performed on mRNA libraries extracted from a mixture of whole plants and fungi at different time points post infection (0–96 hpi). Conidia at 0 h and cultured in potato dextrose broth (PDB) for 6 h were used as controls, with each treatment being replicated three times. To differentiate the mixed transcriptomic reads, the clean reads were aligned against the reference genomes of *B. cinerea* B05.10 [25] and *A. thaliana* Col-0 [26] for the attribution of sequences to their respective organisms (Additional file 2: Table S1 and S2).

To validate the reliability of the RNA-seq data and ensure their suitability for further analysis, we performed quantitative real-time PCR (qRT-PCR) validation. We randomly selected eight genes with known roles in plant defense or fungal pathogenesis, including four genes from *A. thaliana* (*AtPR1*, *AtRBOHD*, *AtPDF1.2*, *AtWRKY18*) and four genes from *B. cinerea* (*BcCrh1*, *BcHip1*, *BcXYG1*, *BcIEB1*). As measured by qRT-PCR, the expression patterns of these genes were highly consistent with the RNA-seq data (Additional file 1: Fig. S1), indicating the accuracy and quality of the RNA-seq data for further analysis.

#### Infection pattern of *B. cinerea* at the transcriptional level

To investigate the transcriptional dynamics of both the host and *B. cinerea* during infection, we conducted a principal component analysis (PCA) and correlation analysis on the expression matrices of *A. thaliana* and *B. cinerea*, respectively. The PCA and correlation analysis of *A. thaliana* samples did not show clear clustering patterns at different infection time points (Additional file 1: Fig. S2), which may be attributed to underlying physiological differences between these samples. Consequently, our subsequent analysis focused on immune-related genes in *A. thaliana*. In contrast, the analysis of *B. cinerea* revealed four distinct clustering patterns (S1–S4) between the spore, early, mid, and late infection stages (Fig. 2A and Additional file 1: Fig. S3).

To further validate these transcriptional stages, we quantified *B. cinerea* biomass during the infection process using qRT-PCR (Fig. 2B). As expected, the transcriptomic and biomass analyses generated highly consistent results, confirming the above separation

of distinct infection stages. Moreover, KEGG enrichment analysis of differentially expressed genes (DEGs) at each infection time point relative to the spore stages unveiled the functional divergence of genes across the early, middle, and late infection stages (Fig. 2C). These findings agree with the earlier microscopic observations of conidial invasion (Fig. 1). Based on these findings, we delineated *B. cinerea* infection into four distinct stages: preparation stage S1 (0–6 hpi), initial infection stage S2 (6–12 hpi), expansion stage S3 (12–48 hpi), and late phase (48–96 hpi). These conclusions are consistent with previous studies, and our transcriptome data further elucidates the differences in transcriptional reprogramming at each infection stage.

#### Temporal dynamics of gene expression during gray mold disease progression

To define the temporal changes of fungal gene expression during gray mold development, we analyzed the gene expression patterns across the infection time-series using MFUZZ k-means clustering algorithm [27]. Based on correlation coefficients, we identified nine modules of co-expressed genes in *B. cinerea* (Additional file 1: Fig. S4A), which involved 8030 genes and accounted for 65.9% of the whole genome. Each module displayed distinct expression patterns at different time points, reflecting the dynamic transcriptional landscape throughout the infection process and aligning with the previously defined four stages of *B. cinerea* infection: S1 (M1, M2, M3), S2 (M4), S3 (M5), and S4 (M6, M7, M8, M9) (Fig. 3A).

The M1 and M2 modules, encompassing a total of 1704 genes, exhibited the highest expression in conidia. Gene ontology (GO) and KEGG enrichment analysis suggested that phosphorelay sensor kinase activity and transcription regulators play crucial roles in maintaining spore dormancy and morphology (Fig. 3B and Additional file 1: Fig. S5A). For example, *Bos5* and *BcSln1*, two important components of the HOG signaling pathway, are essential for proper conidiation [28]. The *bos5* mutant displayed sparse mycelium and no conidiation, while the *sln1* mutant produced abundant conidia but lacked sclerotia, under all light conditions [29]. *SKN7*, a downstream transcription factor in the HOG pathway, plays a crucial role in spore development and stress responses. Deletion of *skn7* in *B. cinerea* led to fewer sclerotia, no conidia, and higher sensitivity to H<sub>2</sub>O<sub>2</sub> [30]. Furthermore, the VELVET protein *VEL1* is involved in regulating spore development. In the *vel1* deletion mutant, mycelial and conidiation melanization increased, while hyphal growth, sclerotial formation, and sporulation decreased [31].

The genes associated with germ tube formation and appressorium-mediated infection were predominantly clustered within M2 and M3, showing peak expression

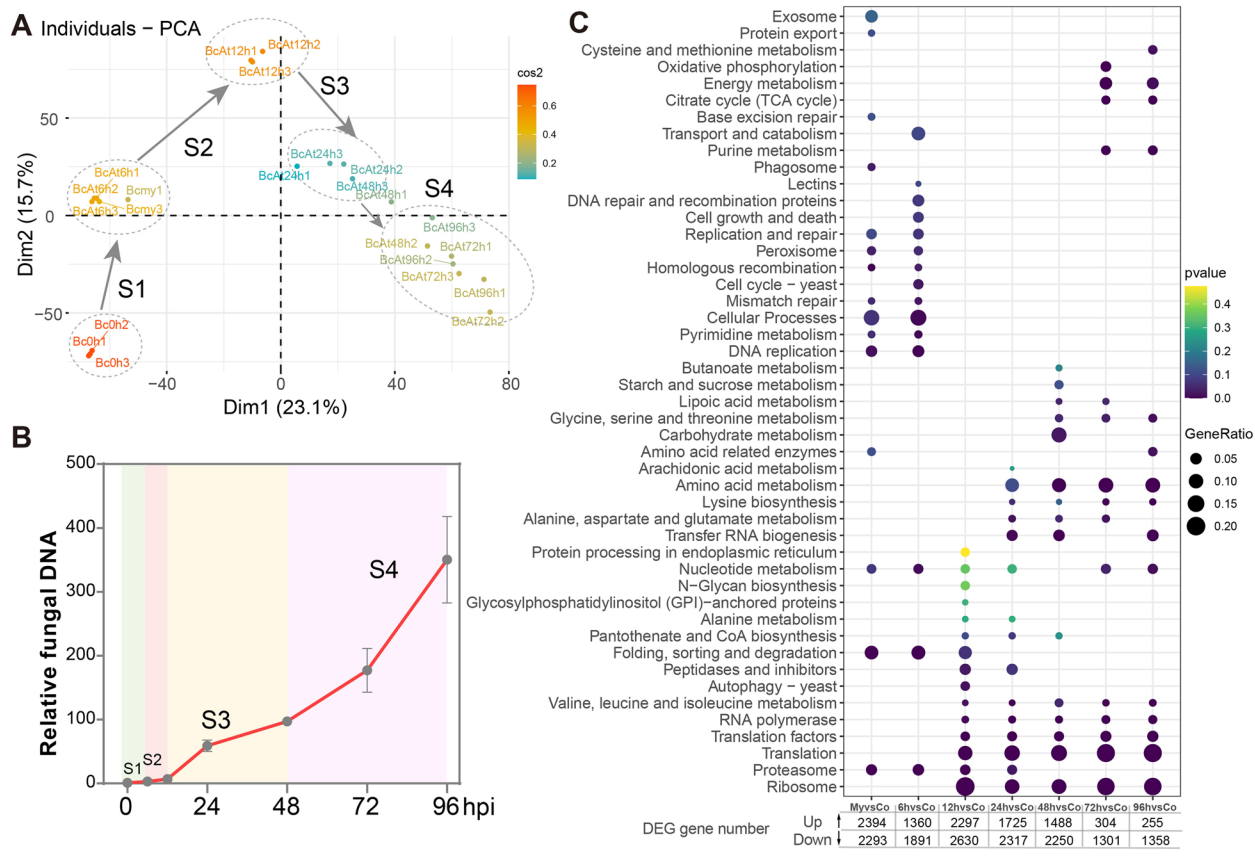


**Fig. 2** Dynamics of *B. cinerea* transcripts and fungal biomass during infection of *A. thaliana*. **A** PCA of RNA-seq data from *B. cinerea* during colonization of *A. thaliana*. Each point represents one of three biological replicates per time point. **B** Quantification of fungal biomass based on genomic DNA. qRT-PCR was performed using *A. thaliana*-specific (*Actin2*) and *B. cinerea*-specific (*Actin2*) primers with the same infected plant material. Data points represent the mean ratios of fungal DNA to plant DNA ( $2^{\Delta\Delta Ct}$ ). Error bars indicate the standard deviation (SD) of three biological replicates. **C** KEGG pathway comparison of DEGs at different infection time points compared to *B. cinerea* conidia

at 6 hpi (Fig. 3A). These two modules contained 1859 highly expressed genes. GO and KEGG enrichment analysis indicated this stage is primarily linked to DNA replication, RNA binding, and hydrolytic protease activity (Fig. 3B and Additional file 1: Fig. S5A), which signifies the initiation of spore germination and appressorium development. For example, *BcCyp2* does not affect mycelial growth, but delays conidial germination and germling development [32]. The septin protein *SEP4*, also present in this module, facilitates host infection by affecting appressorium formation through turgor pressure [33].

The genes in M4 marked the initial colonization of plant tissues and reached the highest expression at 12 hpi. GO and KEGG enrichment analysis of M4 cluster genes revealed that they are associated with phosphatase activity and protein secretion (Fig. 3B and Additional file 1: Fig. S5A). Kinases BMP3 and *BcMkk1* are important components of the MAPK-associated CWI pathway, which regulates virulence by participating in the regulation of tolerance to reactive oxygen species (ROS) [34, 35].

Additionally, *BcSec14* and *BcSec31*, which are probably involved in mediating the secretion of vesicle-associated proteins, facilitate the establishment of infection [36].

M5 comprised 632 genes involved in invasive hyphal growth, including those associated with tolerance to ROS and secretion of catalytic enzymes (Fig. 3B). In *B. cinerea*, aquaporins (AQPs) are crucial H<sub>2</sub>O<sub>2</sub> transporters, deletion of *aqp8* impairs growth, conidiation, and sclerotia formation [37]. Additionally, thioredoxins, such as Trx1, play a role in mitigating oxidative stress by reducing H<sub>2</sub>O<sub>2</sub> accumulation [38]. The phytotoxin botrydial, which induces necrotic lesions in hosts, is only secreted by *B. cinerea* [39]. Notably, the P450 monooxygenases Bot1, Bot2, Bot4, and Bot6, which are involved in botrydial biosynthesis, are present in the module M5.

M6 included genes upregulated at 48 hpi, which coincides with the increase in fungal biomass and lesion expansion. This module was enriched in genes encoding hydrolytic enzymes, including various hydrolases and pectin esterases (Fig. 3B). Notably, several of these

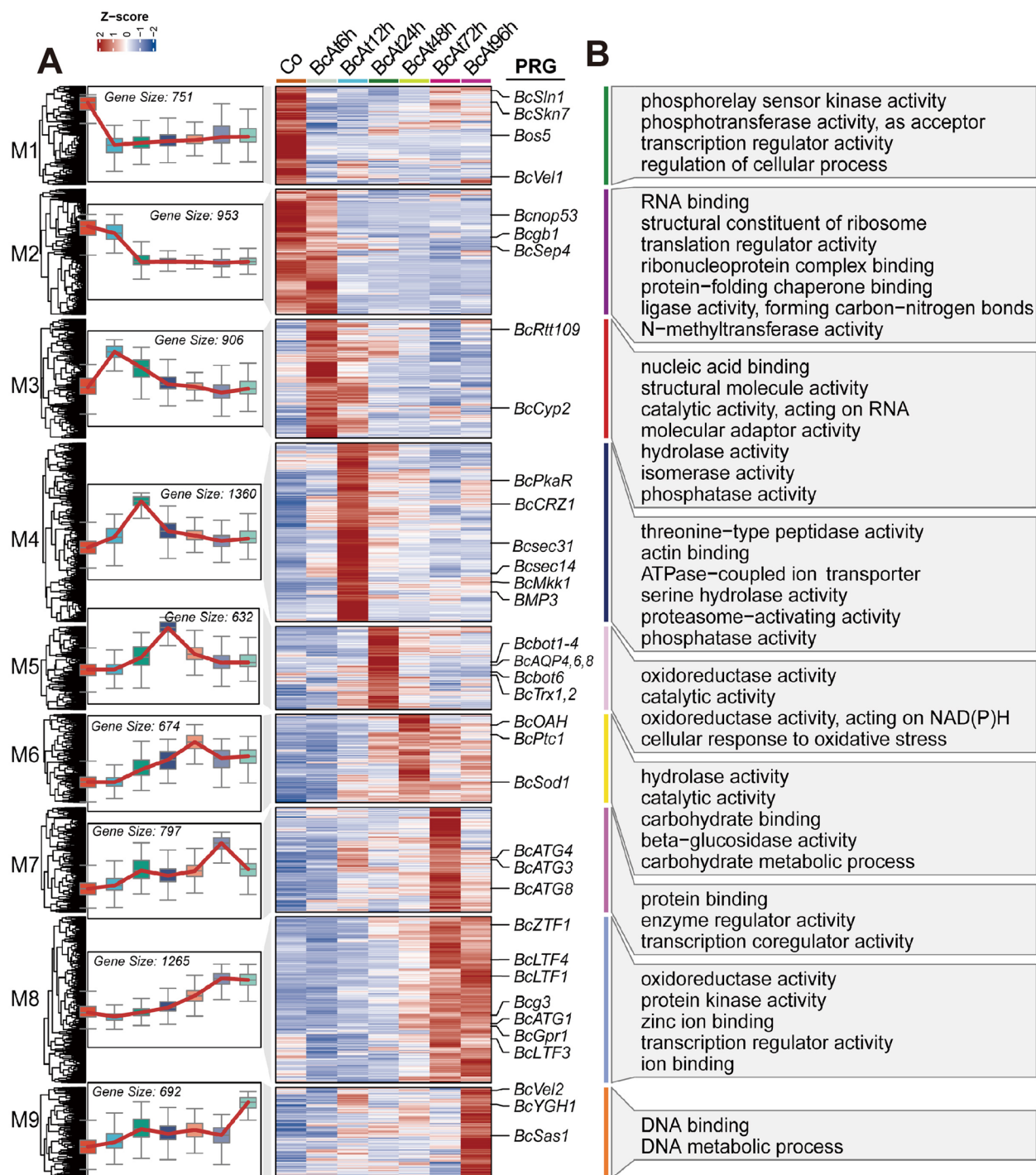


**Fig. 3** Dynamic clustering and functional enrichment analysis of DEGs in *B. cinerea* during the infection time course. **A** Heatmaps displaying the hierarchical clustering of DEGs from each co-expression module in *B. cinerea*. PRG pathogenicity-related genes in *B. cinerea*. **B** GO molecular function (MF) enrichment analysis for each co-expression module in *B. cinerea*. The figure displays the results of g:Profiler enrichment analysis, highlighting the top 8 enriched GO terms

enzymes, such as BcPG1, BcSpl1, BcXYG1, BcNEP2, and BcHip1, have been reported to act as CDIPs [12, 40–42] and probably contribute to the induction of plant cell death and promotion of lesion expansion.

M7, M8, and M9 represented the late stages of *B. cinerea* infection, and the genes were characterized by high expression levels at 72 and 96 hpi. This stage is marked by the upregulation of genes associated with

conidiophore development and conidiation, leading to the production and dissemination of new spores, thereby completing the fungal life cycle and perpetuating the disease cycle. Notably, these modules were enriched in genes encoding transcription factors and signaling proteins involved in regulating sclerotial and conidial differentiation. These modules included four G-protein coupled receptors (GPCRs): Bcg3 and BcGpr1–3 [43], which play important roles in sensing environmental cues and triggering downstream signaling cascades. Additionally, light-regulated transcription factors BcLTF1, BcLTF3, BcLTF4, and BcZTF1 [44–46] were present in these modules, suggesting a role of these genes in light sensing to regulate conidial formation. Moreover, some autophagy-related genes, including *BcATG1*, *BcATG3*, *BcATG4*, and *BcATG8*, were found within these modules. These genes have been previously identified to be associated with the vegetative differentiation and pathogenicity in *B. cinerea* [47–50], suggesting the potential role of autophagy at the late stages of lesion expansion and sporulation.

#### Expression patterns of genes involved in defense responses of *A. thaliana*

To investigate the overall gene expression patterns during the infection process, we clustered the 16,036 identified DEGs, which represented 65.9% of the entire genome, using the MFUZZ k-means clustering algorithm [27]. As a result, these DEGs were divided into eight clusters named as C1 to C8 (Additional file 1: Fig. S4B). The heatmap of these eight clusters revealed significant shifts of gene expression (both up- and down-regulation) at different time points (Fig. 4A). Subsequently, we performed GO and KEGG enrichment analysis on each cluster to investigate their functions (Fig. 4B and Additional file 1: Fig. S5B).

In cluster C1, 2640 genes were downregulated after *B. cinerea* infection, which were primarily enriched in metabolism-related functions, suggesting an initial metabolic reprogramming in response to pathogen perception to coordinate plant growth and defense. In contrast, clusters C2 and C3, which together contained 3648 genes, were significantly upregulated at 6 hpi. Despite limited enrichment of KEGG pathway, GO analysis revealed enrichment of protein and carbohydrate synthesis, indicating activation of defense-related processes. Notably, the genes involved in ethylene (ET) biosynthesis and signaling, such as *ACS2* and *RAP2.2*, were enriched in these clusters, highlighting the role of ET-mediated defense against *B. cinerea* [51, 52].

In cluster C4 with 1909 genes, the gene expression reached the peak at 12 hpi. GO and KEGG analysis indicated enrichment of genes associated with signaling pathways, particularly the MAPK signaling pathway. At

this stage, plants sense the pathogen invasion and begin to utilize their innate immunity to resist the pathogen. Notably, cluster C4 also contained a significant number of genes previously reported to confer resistance to *B. cinerea*, including *PEN1*, *RBOHD*, *EBF2*, *MPK3*, *ACS6*, *ERF5*, *JAZ1*, and *PAD3* [51, 53–58]. These results further supported the crucial role of cluster C4 in plant defense mechanisms against *B. cinerea*.

Cluster C5 showed high expression at 12, 24, and 48 hpi. GO and KEGG analysis suggested the involvement of these genes in processes such as ion binding, catalytic activity, lipid transport, and protein transport. During this medium stage of *B. cinerea* infection, plants utilize various pathways to defend against the pathogen invasion. Notably, this cluster included genes such as cytochrome P450 monooxygenase 71A13 (*CYP71A13*), which is known to control camalexin synthesis and contribute to the resistance of *A. thaliana* to *B. cinerea* [59]. Moreover, *ERF1* and *WRKY33* are respectively involved in JA/ET and ABA signaling pathway-mediated defense against *B. cinerea* [56, 60].

In clusters C6 and C7, the gene expression reached the peak at the later stages of *B. cinerea* infection (48–96 hpi). Go and KEGG analysis revealed enrichment in processes related to energy metabolism, oxidative processes, and leucine-rich repeat (LRR) proteins, suggesting a shift towards defense and repair mechanisms. Notably, these clusters contained genes such as *ATG18a* involved in autophagy regulation and known to attenuate resistance against necrotrophic pathogens such as *B. cinerea* [61]. Additionally, *EDS1*, which promotes *B. cinerea* infection by regulating the hypersensitive response (HR) [62], is also present in the C7 cluster.

In cluster C8, the genes were continuously upregulated throughout the infection process. This cluster included key players in plant defense against *B. cinerea*, such as *BIK1*, a cytoplasmic receptor-like kinase essential for basal immunity. Additionally, the cluster contained genes involved in the MPK6-mediated phosphorylation of ERF72, a process that contributes to resistance to *B. cinerea* by directly or indirectly activating the transcription of camalexin biosynthesis enzymes [55, 63].

To further investigate the defense response of plants, we analyzed the expression patterns of genes involved in key defense pathways, including hormonal signaling salicylic acid (SA), jasmonic acid (JA), ET, MAPK signaling, CNL and TNL resistance genes, callose deposition, phytoalexin biosynthesis, MYB and WRKY transcription factors (Additional file 1: Fig. S6). Although SA is typically associated with defense against biotrophic pathogens and JA/ET signaling is related to defense against necrotrophic pathogens [64], this study revealed complex interplays of these pathways in resistance against *B. cinerea* infection.

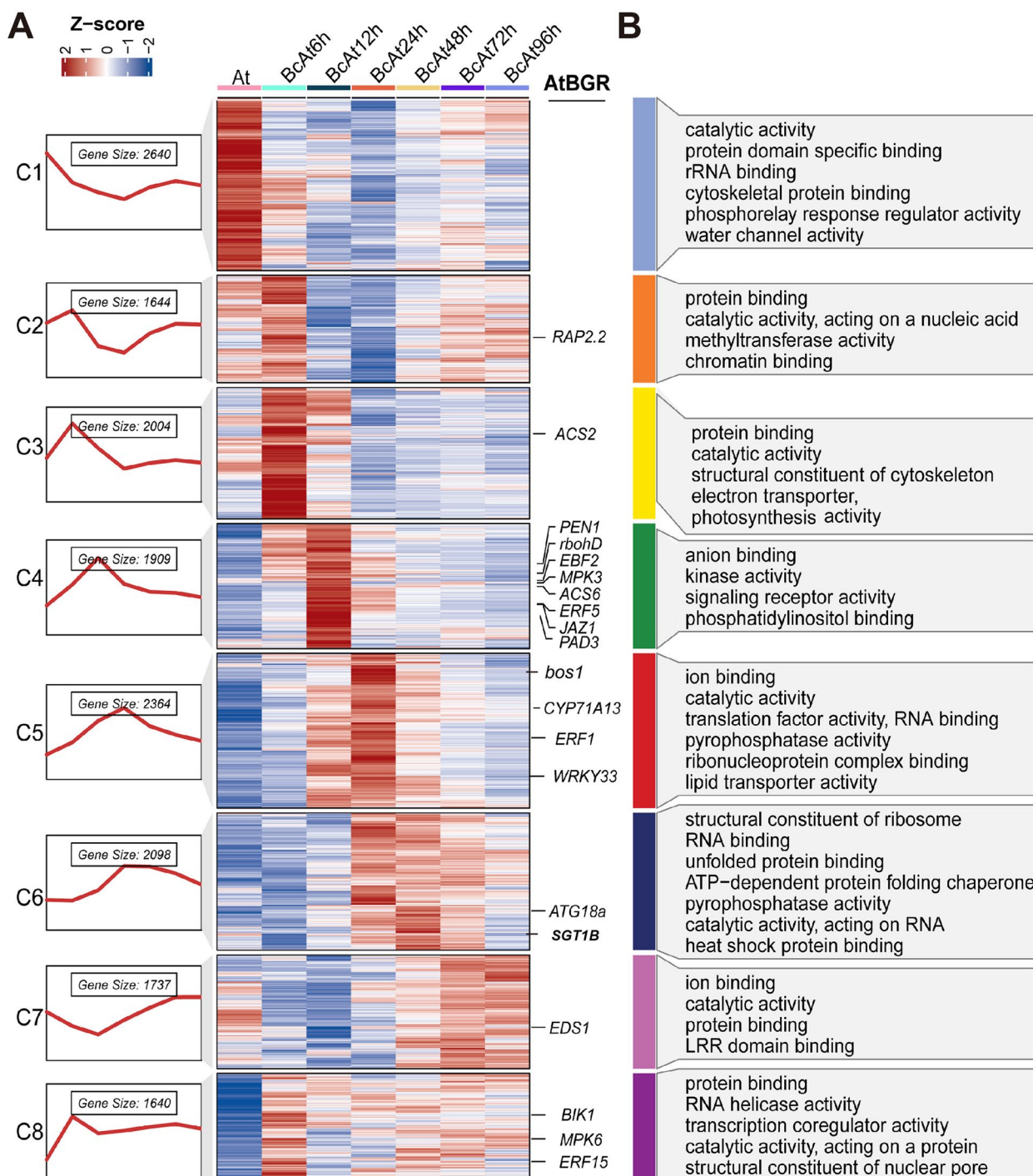


**Fig. 4** Dynamic clustering and functional enrichment analysis of DEGs in *A. thaliana*. **A**, Heatmaps displaying the hierarchical clustering of DEGs from each co-expression module in *A. thaliana*. AtBGR *A. thaliana* genes for resistance to *B. cinerea*. **B**, GO molecular function (MF) enrichment analysis for each co-expression module in *A. thaliana*. The figure displays the results of g:Profiler enrichment analysis, highlighting the top 8 enriched GO terms.

Numerous SA-responsive genes, such as *PR1*, *PR3*, *PR4*, and *PR5*, were upregulated during the mid to late stages of infection. Similarly, JA/ET-responsive genes, including

*JAZ1* (a JA signaling repressor), *OPR1* (involved in JA biosynthesis), *ACO1* (a key enzyme in ethylene biosynthesis), *EIN3* (a central ethylene signaling transcription

factor), and *EDF1* (an ERF transcription factor regulating ethylene-responsive genes), showed increases in expression during the mid-stages of infection [57, 65, 66]. These results suggest that multiple signaling pathways are modulated, either directly or indirectly, during *Arabidopsis*'s resistance response to *B. cinerea*.

In addition, plants can produce callose and phytoalexins to defend against pathogen invasion. Expression cluster analysis revealed that most genes involved in the synthesis of phytoalexins and callose probably play crucial roles during the early stages of *B. cinerea* infection (6 and 12 hpi). For example, the callose synthase genes *GLS5* and *GLS8* have been reported to contribute to resistance against pathogen invasion by regulating callose accumulation [67, 68]. Furthermore, *PAD1*, *PAD2*, *PAD3*, and *PAD4*, all of which are involved in phytoalexin biosynthesis, showed early upregulation. Notably, mutation in any of these *PAD* genes resulted in the inability to synthesize camalexin, leading to reduced resistance against pathogens [58, 69, 70].

The *A. thaliana* genome contains numerous transcription factors that contribute to pathogen resistance, particularly those belonging to the MYB, WRKY, and ERF families. In this study, we observed distinct expression patterns of these families during *B. cinerea* infection (Additional file 2: Fig. S6). WRKY transcription factors, such as *WRKY70*, which is known for its role in integrating SA and JA defense responses [71], exhibited sustained expression throughout the mid to late stages of infection. In contrast, ERF transcription factors, including key regulators of JA/ET signaling such as *ERF1*, *ERF5*, and *ERF6*, displayed a prominent expression peak at the mid-stage, which is consistent with their positive influence on defense against *B. cinerea* [72]. MYB transcription factors, however, did not exhibit a clear or consistent expression pattern across the infection time course.

Based on the analysis of host transcriptional dynamics, we found that numerous genes associated with SA signaling and the WRKY transcription factor family were upregulated at various time points throughout the infection period. In contrast, genes involved in JA and ET signaling pathways were primarily upregulated during the middle stage of infection.

#### Analysis of candidate effector proteins in *B. cinerea*

To explore the potential effectors in *B. cinerea*, we comprehensively analyzed the candidate effector proteins (CEPs) based on their bioinformatic features and expression profiles. By using SignalP 5.0 and TMHMM 2.0 [73, 74], we first identified 852 Botrytis secreted proteins (BSPs) in the *B. cinerea* proteome, which were characterized by the presence of signal peptides and absence of transmembrane domains. Subsequent time-series analysis with the Mfuzz algorithm clustered 656 of these BSPs into seven distinct

groups based on their similarities in expression pattern (Fig. 5A). Notably, 17 previously reported CDIPs were identified in the analyzed clusters. For instance, The Nep1-like proteins (NLPs) BcNep1 and BcNep2 [42], with peak expression at 6 and 48 hpi, respectively, trigger plant cell death through the accumulation of H<sub>2</sub>O<sub>2</sub> in chloroplasts. Similarly, *BcCrh1* [75] and *BcCrh4* [76], with peak expression at 12 hpi, induce both plant cell death and immune responses, independent of their transglycosylase activity.

The M5 module included *BcPLP1*, which shares homology with the effector VmE02 from *Valsa mali* [77]. In *V. mali*, VmE02 is recognized by the plant receptor RE02 to trigger a defense response that promotes cell death [78], suggesting that *BcPLP1* may play a role in modulating host cell death in *B. cinerea*. Notably, the M6 module included the largest number of known CDIPs (BcSpl1, BcNep2, BcXyn11A, BcHip1, BcPG1, and BcXYG1) [12, 40–42, 79], suggesting deployment of many effector proteins with cell death-inducing activity at the 48 hpi to facilitate infection and overcome plant defenses. Finally, BcSSP2 [80], a cytotoxic effector expressed at the late infection phase, exhibited the highest expression at 96 hpi in this study.

To gain more insights into the potential functions CEPs, we performed comprehensive functional annotation and carbohydrate-active enzyme (CAZyme) analysis using HMMER [81] and the dbCAN3 [82] database. The results revealed a diverse functional landscape of BSPs, with 285 BSPs being lack of any annotated function or carbohydrate activity (CAZymes), possibly indicating the presence of novel effectors with yet undiscovered roles in the infection process. Among the 567 BSPs with predicted functional domains, 248 were identified as CAZymes (Fig. 5B). Notably, the majority (151) of these CAZymes belonged to the glycoside hydrolase (GH) class and participated in every stage of infection (Additional file 1: Fig. S7B).

To identify potential effectors within the predicted CAZymes and non-CAZyme BSPs, we employed two distinct prediction algorithms: EffectorP 3.0 and DeepRedEff [83, 84]. By combining the outputs of both algorithms, we generated 591 candidate effector proteins (CEPs). Among the secreted enzymes, 181 (69.1%) were classified as CEPs, while 410 (69.5%) of the non-enzymatic proteins were designated as CEPs (Fig. 5C). The proportion of CEPs between the two groups was not significantly different. Therefore, CEPs in this study were defined as the union of BSPs predicted by EffectorP 3.0 and DeepRedEff. Further analysis revealed that the number of enzymatic CEPs peaked at M6, while the number of non-enzymatic CEPs was higher at the M4, M8, and M9. Notably, only two enzymatic effectors were found at the M4, where the highest number of CEPs was observed, suggesting that a substantial number of effectors might reside within the non-enzymatic CEPs at this stage (Fig. 5D).

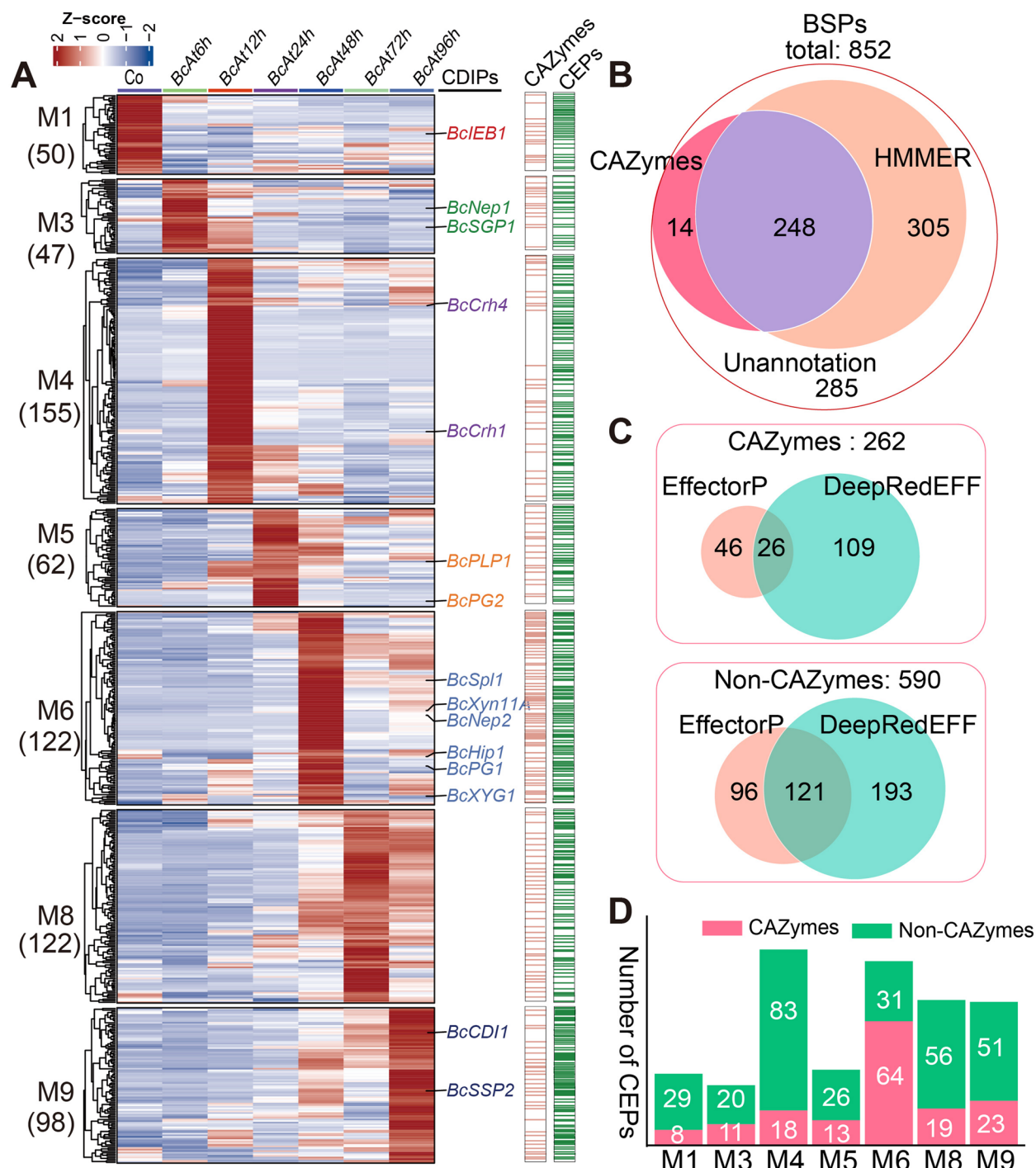


**Fig. 5** Analysis of CEPs in *B. cinerea*. **A** Heatmap illustrating the clustering of *B. cinerea* secreted proteins within each co-expression module. The right panel shows the distribution of CAZymes and CEPs in each cluster. **B** Functional annotation of BSPs. **C** Comparison of CAZymes and non-CAZymes CEPs predicted using EffectorP fungi 3.0 and DeepRedEff algorithms. **D** Numbers of CAZymes and non-CAZymes CEPs in each module

To explore the potential sites of action for these predicted effectors, we analyzed their subcellular localization using WoLF PSORT [85], LOCALIZER [86], and BUSCA

[87]. The majority (146) of *B. cinerea* CEPs were localized to the apoplast, the extracellular space within plant tissues. In contrast, only a small number of them were

predicted to target the cytoplasm (7) and none was predicted to target the nucleus by all three algorithms (Additional file 1: Fig. S7C). This apoplastic localization pattern in *B. cinerea* differed from that observed in hemibiotrophic pathogens like *M. oryzae* [17], which typically secrete a larger proportion of effectors targeting the cytoplasm or nucleus to manipulate host cellular processes.

#### Comparative analysis of CEP orthologs and paralogs

To explore differences in CEPs among pathogens with diverse lifestyles, we selected 25 plant pathogens representing necrotrophic, biotrophic, and hemibiotrophic lifestyles and predicted their CEPs using the method described above. OrthoMCL [88] analysis revealed that necrotrophic and biotrophic pathogens generally possessed fewer CEPs compared to hemibiotrophic pathogens. Notably, most CEPs were found to belong to shared clusters across all three lifestyles, and necrotrophic pathogens, apart from *P. tritici-repentis* and *P. nodorum*, exhibited a lower number of species-specific genes (Fig. 6A).

To delve into the evolutionary relationships among CEPs within *B. cinerea*, we also compared the conservation of CEPs among different species within the *Sclerotiniaceae* family using MCSanX [89] and BlastP [90]. The results showed that most CEPs are conserved within the *Sclerotiniaceae* family, with each species possessing fewer than 50 species-specific CEPs (Fig. 6B). These findings suggest that these CEPs may play important roles in the evolution of *Sclerotiniaceae* species.

Further investigation into the genomic distribution of 591 CEP genes revealed their presence across 16 *B. cinerea* chromosomes, excluding chromosomes 17 and 18. Notably, these genes generally do not exhibit a specific preference for particular chromosomal regions, although several known CDIPs, including BcXyn11A, BcSpl1, BcCDI1, BcNEP1, were located near telomeric regions (Fig. 6B and Additional file 1: Fig. S8). This distribution differs from the effector localization patterns observed in other pathogens, such as *M. oryzae* and *L. maculans*, which tend to cluster near the sub-telomeric regions of chromosomes [91].

#### Structural conservation of CEPs during *B. cinerea* infection

With the rapid development of structural biology, there has been growing evidence revealing different degrees of structural conservation among secreted effector proteins in plant pathogens [22]. For instance, in the rice blast fungus *M. oryzae*, the MAX effectors share a common β-sandwich fold, although they lack sequence similarity [17, 23]. Inspired by these studies,

we investigated whether CEPs exhibit similar structural conservation during *B. cinerea* infection.

We retrieved the 3D structures of all 591 CEPs from the AlphaFold2 database [92] and expanded the analysis to include known effector proteins from other fungal species (Additional file 16), including Avr-PiK, AVR-Pia, and AVR-Piz-t from *M. oryzae* [93], AvrLm4-7 and AvrLm5-9 from *L. maculans* [94, 95], ToxA and ToxB from *Pyrenophora tritici-repentis* [96, 97], and ECP10-1 from *Cladosporium fulvum* [98]. Subsequently, we selected CEPs with pLDDT  $\geq 50.00$  and performed structural clustering using the Foldseek [99] to identify groups of CEPs with similar structural features. Surprisingly, none of *B. cinerea* CEPs was clustered with these known effector proteins. We found that 214 CEPs possessed at least one structurally similar counterpart, which could be classified into 76 clusters in terms of structure, while the remaining 377 CEPs were singletons (Additional file 1: Fig. S9 and Additional file 13: Table. S12). This result was different from sequence similarity analysis, which identified 214 CEPs with at least one similar sequence and 376 singletons. Combined analysis revealed that only 136 CEPs exhibited both sequence and structural similarities (Fig. 6B). These results suggested a notable degree of structural conservation among *B. cinerea* CEPs. Furthermore, the previously characterized CDIPs, BcCDI1, and BcIEB1, which lack of any recognizable Pfam domains and share no sequence similarity, exhibited structural similarities with a TM-score of 66.8% (Additional file 1: Fig. S10).

We then selected the top 13 largest structural clusters and analyzed their relationship with the previously defined temporal expression modules (Fig. 7A). In most cases, structurally conserved proteins are expressed in M4–M9 (12–96 hpi). Notably, structural clusters C4 and C8 are over-represented in M6 and M4, respectively, and are predicted to be glycosyl hydrolases and serine proteinase pro-kumamolisin. Structural C1, C2, and C3 are more evenly distributed across M5, M6, and M8, which are primarily composed of lipase, carboxylesterase, FAD-binding domain proteins, and royal jelly proteins (Fig. 7B). These findings suggest a strong link between structural conservation among CEPs and their co-expression during *B. cinerea* infection.

#### Identification of novel *B. cinerea* CEPs inducing or suppressing plant cell death

Based on our previous analyses, we selected 66 CEPs for experimental validation of their potential roles in modulating plant cell death. These included 40 with predicted carbohydrate activity, 20 with uncharacterized functions, and 6 *B. cinerea*-specific CEPs. The selected CEPs were distributed across the infection stages: 25 from the

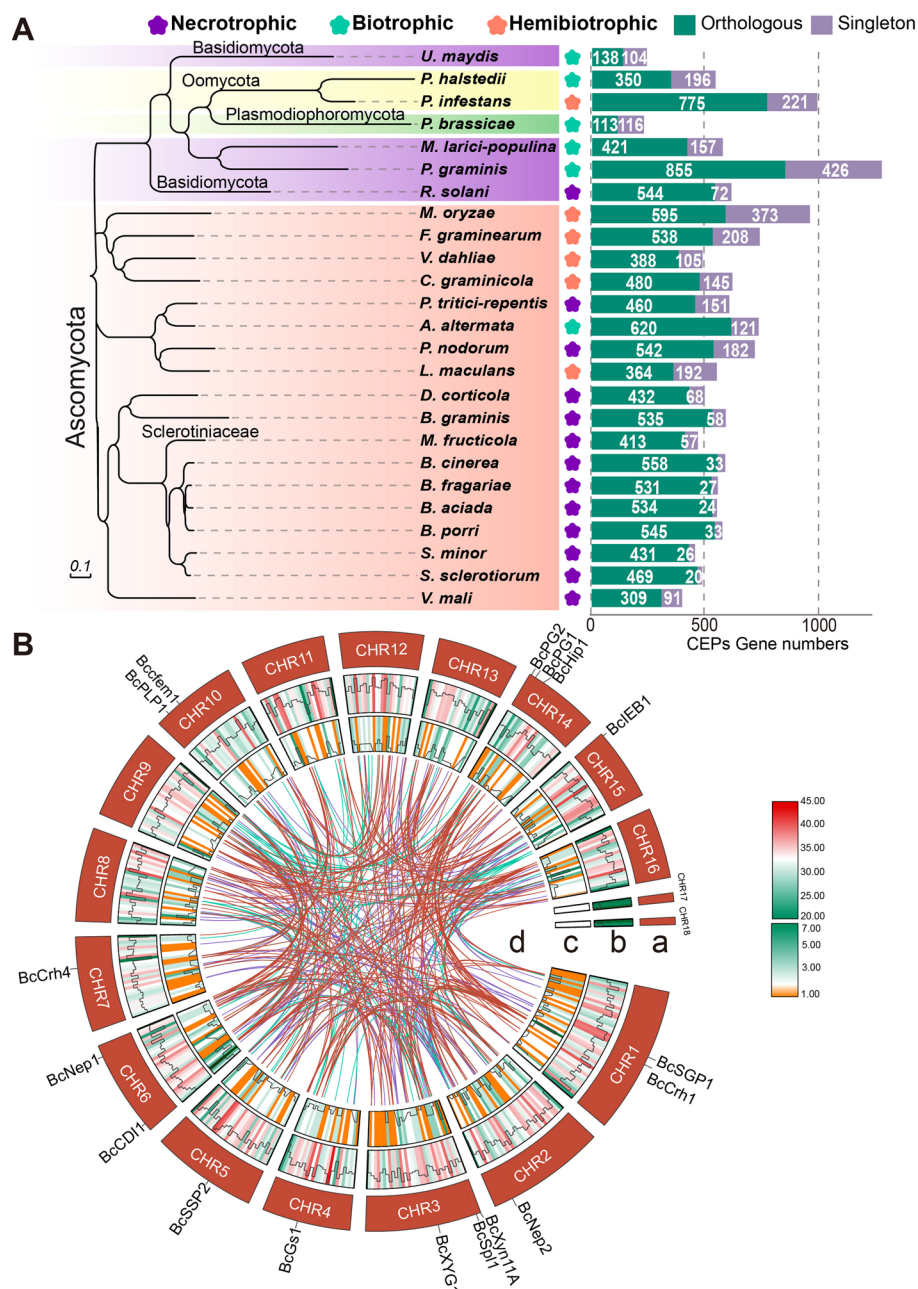


**Fig. 6** Analysis of orthologs and paralogs for CEPs in *B. cinerea*. **A** Species tree based on CEPs. The 25 species in this study are divided into three classes: Mastigomycota, Basidiomycota, and Ascomycota. CEPs from these species were clustered based on protein sequence similarity. Clusters containing members from multiple species are categorized as “Orthologous”, while proteins that do not cluster with any other protein are labeled as “singleton”. **B** Circos plot displaying information on CEPs. **a** Backbone of the 18 chromosomes. **b** Gene density of all genes across the genome. **c** Gene density of CEPs. **d** Collinearity relationships within the *B. cinerea* genome. Purple lines (connecting 78 genes) indicate collinearity among the amino acid sequences of the CEPs. Green lines (connecting 95 genes) indicate collinearity among 3D structures of the CEPs. Red lines (connecting 136 genes) indicate collinearity of both amino acid sequences and 3D structures

early stage, 30 from the middle stage, and 11 from the late stage (Additional file 14: Table S13). We successfully cloned 48 CEP genes into a binary PVX vector for transient expression in *N. benthamiana* via *Agrobacterium tumefaciens*-mediated transformation (ATMT).

To assess their ability to induce or suppress plant cell death, we expressed each of the 48 CEPs separately or together with the mouse pro-apoptotic protein Bax in *N. benthamiana*. Surprisingly, no CEP demonstrated the ability to suppress BAX-induced cell death (Fig. 8A).

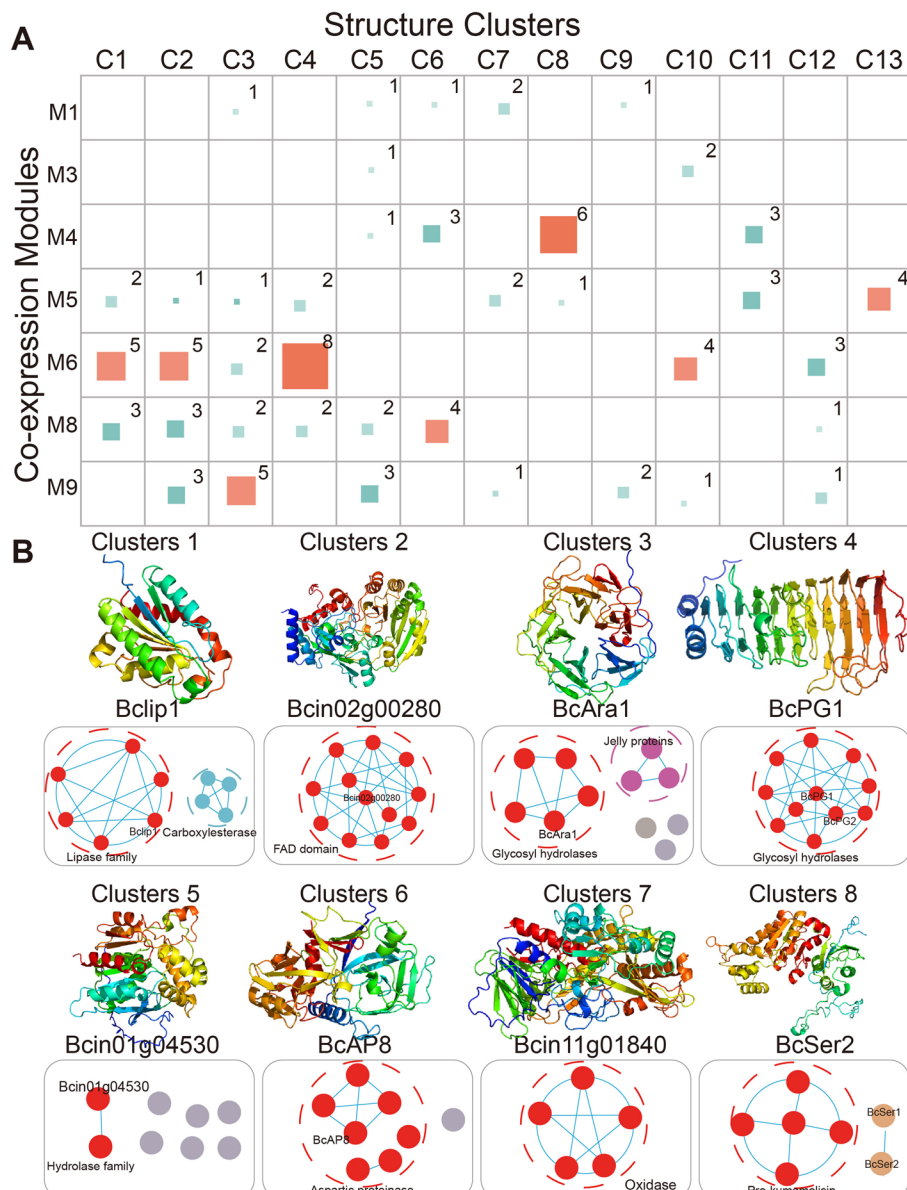


**Fig. 7** Comparison analysis of structurally conserved and temporally co-expressed *B. cinerea* CEPs. **A** Dot plot showing the correspondence between co-expression clusters and the top 13 structural clusters of CEPs. **B** Representative structures and sequence similarity networks for *B. cinerea* CEP clusters 1–8. Top row: predicted structures of representative protein from each conserved structural cluster. Bottom row: sequence similarity networks for proteins within each corresponding structural cluster. Each dot represents a protein; circled dots indicate proteins belonging to the same protein family

Through multiple independent experiments, we identified six CEPs that weakly induced cell death, while five CEPs (S20, S26, S30, S31, and S40) that strongly induced cell death in *N. benthamiana* leaves (Fig. 8B). Notably, the transglycosylase BcCrh4 (S26), the glycoside hydrolase BcXYG1 (S40), and the *V. mali* VmE02 homolog BcPLP1 (S20) were also recently reported to induce cell death and act as PAMPs [76, 78]. However, S30, a *B. cinerea*-specific gene encoding a 94-amino acid protein and S31,

with two transcripts and a GOLD domain, were identified as cell death inducers in this study, but they were not found to have such functions in other pathogens. Further investigation is warranted to elucidate the mechanisms by which S30 and S31 trigger cell death and their specific contribution to *B. cinerea* virulence.

In summary, our results revealed that among the 48 tested CEPs, no CEP exhibited the ability to inhibit Bax-induced cell death. However, we identified five CEPs with

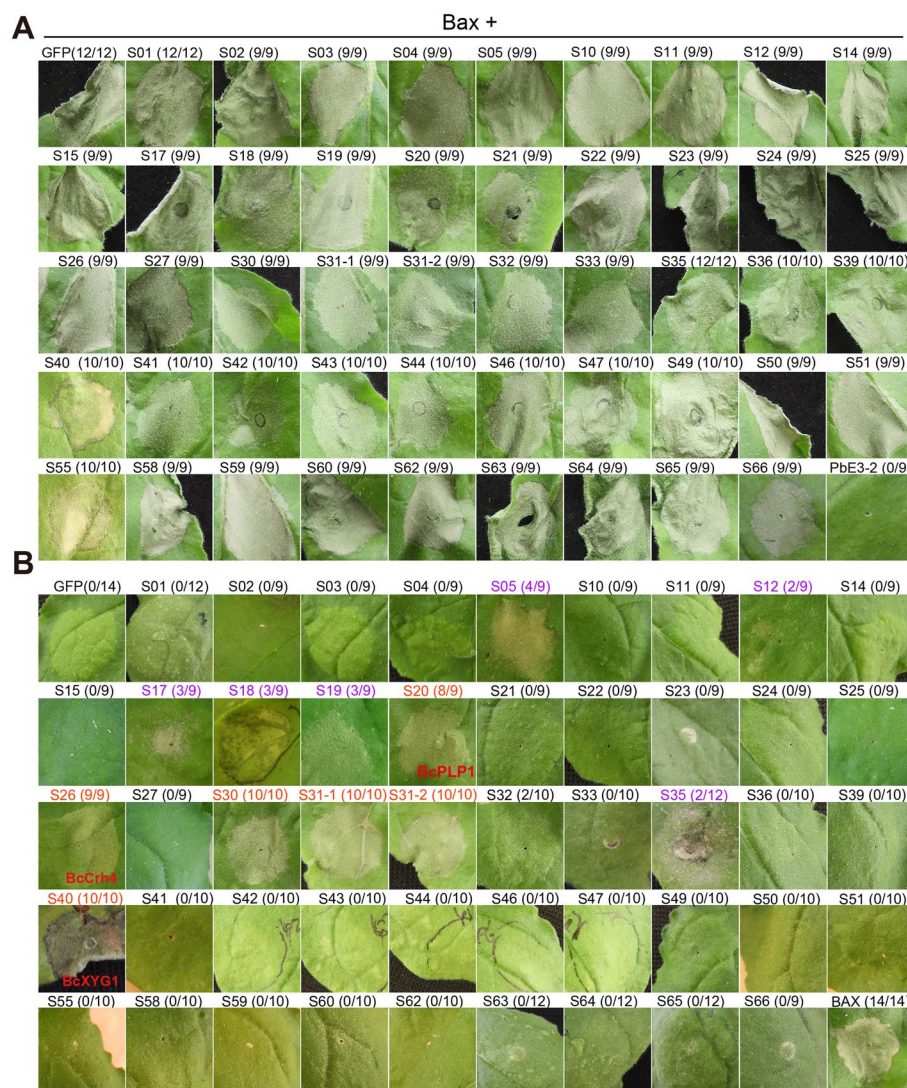


**Fig. 8** Screening for suppressors and CDIPs from *B. cinerea* CEPs. **A** Screening for suppressors. A total of 48 CEPs (S1 to S66) were co-expressed with Bax in *N. benthamiana* leaves to identify CEPs that can suppress Bax-induced cell death. PBE3-2 [100] served as positive control, and GFP was used as a negative control. Images were taken at 5 dpi. **B** Screening for CDIPs. The same 48 CEPs were tested using *Agrobacterium*-mediated transient expression in *N. benthamiana* leaves. BcXYG1 and Bax served as positive control, and GFP was used as a negative control. Purple font indicates weak cell death induction (6 CEPs), and red font indicates strong cell death induction (5 CEPs). Images were taken at 5 dpi

strong cell death-inducing activity, including two previously uncharacterized proteins. Further research is needed to unravel the molecular mechanisms underlying the cell death-inducing activity of these CEPs and their roles in the complex interplay between *B. cinerea* and its host plants.

## Discussion

The mechanisms underlying the rapid infection and disease development caused by *B. cinerea* remain poorly understood [4, 6, 9]. Previous studies have been primarily focused on the developmental and pathogenic processes of *B. cinerea*, particularly mycelial growth, sclerotial

formation, sporulation, appressorium and infection cushion development, and the identification of CDIPs. These studies have revealed the significant roles of signaling pathways, DHN melanin, the *B. cinerea*-specific secondary metabolite phytotoxin botrydial, ROS, and PCWDEs in the pathogenesis of *B. cinerea* [2, 34, 44, 45, 101–107]. However, our understanding of the overall infection process of *B. cinerea* remains incomplete. Hence, we conducted a transcriptomic analysis of the infection process of *B. cinerea* to elucidate the fundamental changes occurring in both the pathogen and the host plant during disease progression. Based on this analysis, we aimed

to identify how the effector proteins of *B. cinerea* are deployed throughout the infection process.

Recent comprehensive studies of *B. cinerea* have focused on transcriptomic analysis of infection cushion formation at a single time point [108], revealing the crucial roles of certain genes in this process. More recently, Bai et al. revealed a dynamic arms race between strawberries and *B. cinerea* during the asymptomatic infection stage (0–12 hpi) [21]. This dynamic interaction highlights the possibility that *B. cinerea* represses host autophagy during the asymptomatic infection stage, potentially linked to the regulation of apoptosis. These data provide a basis for future identification of inhibitors used by *B. cinerea* to suppress host autophagy, furthering our understanding of how *B. cinerea* evades plant defense mechanisms during its early stages of infection. Additionally, Oliver et al. revealed the regulatory network underlying *Arabidopsis*' defense response to *B. cinerea* using microarray analysis of transcriptional reprogramming [109]. Although previous studies have offered valuable insights, there is a clear need for more research investigating the longer-term dynamics of *B. cinerea* infection. Therefore, we combined microscopic observations with dual RNA-Seq to investigate the early, middle, and late stages of *B. cinerea* infection in *A. thaliana*, aiming to elucidate how the pathogen and host plant respond to each other.

We divided four stages of *B. cinerea* infection in *A. thaliana* based on microscopic observations and transcriptome analysis: early (S1 and S2), middle (S3), and late (S4) stage. These findings align with the general understanding of *B. cinerea* infection process, as described by Bi et al. [4]. Here, our study provides further insight into these processes at the transcriptional level. During the S1 stage (0–6 hpi), *B. cinerea* spores germinate without eliciting a host plant response. In the S2 stage (6–12 hpi), *B. cinerea* likely deploys effector proteins to suppress host immune, as evidenced by the enrichment of GO terms related to endoplasmic reticulum, peptidases and inhibitors, and RNA polymerase (Fig. 3). As we know, effector sRNAs act as “cluster bombs” to silence immunity-related genes [16, 110]. These enrichments potentially indicate that *B. cinerea* can also secrete proteins as inhibitors to suppress plant immune responses. During the S3 stage (12–48 hpi), the number of DEGs is the highest for both the pathogen *B. cinerea* and the host *A. thaliana*, accounting for 33.2% and 39.7% of the total DEGs, respectively (Figs. 3 and 4). Most of the previously reported CDIPs are also highly expressed in this stage, suggesting that the battle between *B. cinerea* and *A. thaliana* is most intense at this stage. In the S4 stage (48–96 hpi), *B. cinerea* establishes a successful infection while maintaining high expression of genes involved in DNA replication and repair,

autophagy, and MAPK signaling pathway. We speculate that at this stage, the invading hyphae are preparing to form conidiophores. Although we only observed aerial hyphae at 96 hpi (Fig. 1A), the later formation of conidia was not yet involved. The data from this stage also provide potential value for understanding the regulation of conidia formation. This comprehensive understanding of the infection process lays a solid foundation for further experimental investigation to elucidate the molecular mechanism underlying *B. cinerea* pathogenesis and develop effective disease control strategies.

Recent research has been focused on the identification and characterization of *B. cinerea* effector proteins and their plant targets, but currently, the relevant knowledge remains rather limited. Here, 17 CDIP effectors have been identified in *B. cinerea* [4, 76, 80, 111], indicating the need for a more comprehensive investigation. Furthermore, the functional redundancy among *B. cinerea* effectors, where the deletion of multiple effectors has minimal impacts on the pathogenicity, underscores the importance of identifying key effectors that drive the infection [112, 113]. To address this challenge, we conducted a comprehensive time-series analysis of 852 *B. cinerea*-secreted proteins. The results revealed that 77.01% (656) of these secreted proteins exhibited dynamic expression during infection, indicating their potential roles in the pathogenesis of *B. cinerea*. By comparing pathogens with different lifestyles, *B. cinerea* shows a high proportion of orthologous CEP genes, which may reveal the reason for its wide host range. Moreover, subcellular localization analysis demonstrated that the majority of *B. cinerea* CEPs are of an extracellular localization, which is a distinct characteristic relative to the effectors of biotrophic and hemibiotrophic pathogens.

Identification of fungal effectors is challenging due to the lack of conserved sequence similarity and specific motifs, which is different from the RXLR motif found in many oomycete effectors [114]. While fungal effector proteins often lack sequence similarity and characteristic motifs, there are certain similarities in structure. For example, the MAX family effectors in *M. oryzae* exhibit a minimal sequence homology but share a common β-sandwich fold in structure [21, 92]. In this study, we conducted a comprehensive cluster analysis of 591 *B. cinerea* CEPs based on both sequence and structure. Although 214 CEPs had at least one protein with sequence similarity, more CEPs (231) exhibited at least one structurally similar protein, indicating a high degree of structural conservation among *B. cinerea* CEPs. Furthermore, we compared the top 13 CEP structural clusters with the gene modules co-expressed at different infection stages. These results not only provide a rich resource of CEPs for functional analysis but also suggest that the investigation

of co-expressed genes combined with structural prediction and temporal expression profiling may be a powerful approach to identify novel functions of effectors.

PCD, including autophagy and apoptosis, is a critical process in plant-pathogen interactions and plant development [115]. *B. cinerea*, a necrotrophic pathogen, may also exhibit a transient biotrophic phase, and it precisely regulates host cell PCD to facilitate infection. In tobacco, *EDS1* and *SGT1* positively regulate cell death. *EDS1* and *SGT1* mutants are more susceptible to biotrophic pathogens but more resistant to *B. cinerea* [62]. In *A. thaliana*, the botrytis-susceptible1 (*bos1*) mutant, which exhibits impaired cell death spreading, is more susceptible to *B. cinerea* [116]. These findings underscore complex roles of PCD in plant-pathogen interactions. However, the precise mechanisms by which *B. cinerea* effectors modulate PCD remain largely unknown. To address this knowledge gap, we aim to identify effector proteins that either inhibit or promote PCD.

Currently, the methods for effector identification often rely on gene knockout and construction of expression systems in *N. benthamiana* [13, 117]. Transient expression, known for its rapid and visual screening capability, has been widely adopted in studies of plant pathogens. In this study, we employed this method to identify potential effectors among *B. cinerea* CEPs. Based on the above series of bioinformatics analysis, we selected 48 CEPs and conducted transient expression of them in *N. benthamiana*. Our screening was focused on identifying CEPs that could induce or suppress plant cell death, with suppression of cell death as a proxy for host immune suppression. Surprisingly, no CEPs were found to suppress Bax-induced cell death. This may reflect limitations in our screening method or the limited number of CEPs tested, which might not fully capture the complex interplay between the pathogen and host. Despite this, we still successfully identified eleven CEPs that could induce varying degrees of plant cell death in *N. benthamiana*. Notably, two new CEPs (S30 and S31) exhibited consistent and relatively strong ability to induce plant cell death. S30 is a *B. cinerea*-specific small peptide (only 94 amino acids), while S31 contains a GOLD domain. Interestingly, only S31 in the GOLD domain family displayed the ability to induce cell death. Further investigations are currently underway to elucidate the mechanisms underlying their functions.

## Conclusions

This study provides a comprehensive transcriptome resource for understanding the dynamic interplay between *B. cinerea* and *A. thaliana* during gray mold disease development. Dual RNA-seq analysis across seven time points revealed four distinct stages of *B. cinerea* infection, highlighting the speed and complexity of its pathogenic strategy. A global analysis of 591 *B. cinerea* CEPs revealed

distinct temporal expression profiles and structural conservation patterns, suggesting functional specialization among these proteins. Notably, the heterologous expression of 48 CEPs in *N. benthamiana* confirmed the crucial roles of CDIPs in *B. cinerea* pathogenesis. This study provides valuable information for further understanding the pathogenic mechanisms of *B. cinerea* and the role of effector proteins in facilitating *B. cinerea* infection.

## Methods

### Fungal and plant growth conditions

*B. cinerea* strain B05.10 and *A. thaliana* accession Col-0 were maintained as described previously [109]. Conidia were collected from 15-day-old plate cultures of *B. cinerea* for appressorium development assay and leaf infection. Following inoculation, *A. thaliana* plants were incubated in a growth chamber at 22°C, 90% relative humidity, and a 16-h photoperiod with a light intensity of 180  $\mu\text{mol m}^{-2} \text{s}^{-1}$ .

### Plant infection assays for RNA sequencing and microscope observation

*B. cinerea* conidia were harvested from 15-day-old Potato Dextrose Agar (PDA) plates. For spray inoculation assays, 4-week-old *A. thaliana* plants were sprayed with conidial suspension at  $1 \times 10^5$  spores/mL in 50% (v/v) Potato Dextrose Broth (PDB). Whole infected plants were then harvested at 0, 6, 12, 24, 48, 72, and 96 hpi. To visualize the spore infection process, inoculated samples were stained with WGA-AF488 at each time point following the method described by Redkar et al. [118]. Samples were subsequently observed using confocal microscopy (Leica Application Suite X). All collected samples were immediately frozen in liquid nitrogen for RNA extraction. Each treatment (time point) included three biological replicates. Total RNA was extracted using TRIzol reagent (Vazyme). RNA purity was assessed using a NanoDrop spectrophotometer (Thermo Scientific) to confirm an OD260/280 ratio between 1.8 and 2.2 and further verified by 2% agarose gel electrophoresis, and the RNA integrity was assessed with an Agilent 2100 Bioanalyzer.

### RNA-seq library construction and data analysis

Transcriptome libraries were sequenced on the Illumina HiSeq 2500 platform, generating 150 bp paired reads. After adapter trimming and quality filtering, clean reads were mapped to the reference genomes of *A. thaliana* (GCA\_000001735.1) and *B. cinerea* (GCA\_000143535.4) using HISAT2 (v2.0.4). Gene expression levels were quantified as fragments per kilobase of transcript per million mapped reads (FPKM). Differentially expressed genes (DEGs) between treatment and control groups at each time point were identified using DEGSeq (v1.18.0) with a false discovery rate (FDR) cutoff of  $< 0.05$  and a

$|\log_2(\text{fold change})| > 1$ . GO and KEGG enrichment analyses were performed on DEGs using clusterProfiler (v4.6.2) [119] and g:Profiler (v1.47.0) [120] with a significance threshold of  $P_{\text{adj}} < 0.05$ .

#### Time-series analysis of gene expression

Time-series gene expression data were analyzed using the Mfuzz R package (v2.58.0) [27]. Low-abundance features, defined as those with a count less than 10 in over 90% of samples, were removed prior to analysis. Module size was determined using a soft thresholding approach. Time-series expression profiles of each module were visualized using the R package ClusterGVis (v0.1.1) [121]. For each module, GO and KEGG enrichment analyses were performed with g:Profiler (v1.47.0) [120]. Enriched pathways were identified using a  $q$ -value threshold of  $< 0.05$ .

#### Analysis of CAZyme activities and localization of CEPs

CEPs were identified in the *B. cinerea* proteome by searching for proteins lacking a transmembrane domain as predicted using TMHMM v2.0 [73], and SignalP v5.0 was used to predict whether the protein possesses a signal peptide [74]. CEP genes encoding CAZymes were annotated manually and complemented by de novo prediction using dbCAN3 tools [82]. Functional annotations were predicted using HMMER [81]. The terms “hypothetical protein,” “predicted protein,” and “uncharacterized protein” referred to unannotated proteins.

Effector prediction was performed on CEPs using the EffectorP fungi 3.0 [83] and DeepRedEff (v0.12) [84] algorithms. Subcellular localization prediction of CEPs was carried out using WOLF PSORT [85], LOCALIZER [86], and BUSCA [87] tools. Based on the prediction results, CEPs were manually categorized as apoplastic, cytoplasmic, or nuclear.

#### Analysis of CEP orthologs and paralogs

To investigate the evolutionary relationships of CEPs, we analyzed their orthologs and paralogs across 25 fungal and protista species [122–149]. Genome sequences for all species were retrieved from NCBI GeneBank (Additional file 10: Table S9). CEPs were predicted in each species using previously described methods. Orthologous gene families were identified using OrthoVenn3 [150] with the OrthoMCL algorithm and an e-value threshold of  $1e^{-3}$ . Paralogs within the CEPs were identified using MCScanX [89] with an e-value threshold of  $1e^{-3}$ . The resulting CEP gene density was analyzed and visualized using TBtools v2.085 [151].

#### qRT-PCR

Total RNA was extracted from all samples and reverse transcribed into cDNA using the PrimeScript RT reagent

kit with gDNA Eraser (Takara, Dalian, China). qRT-PCR was performed using SYBR Green II (Takara) on a Light-Cycler 480 system (Roche, Switzerland) according to the manufacturer’s instructions. Primer sequences are listed in Additional file 15 Table S14. Relative gene expression was calculated using the  $2^{-\Delta Ct}$  method with *AtActin2* and *BcActin2* as the reference genes for *A. thaliana* and *B. cinerea*, respectively.

#### Structural clustering and visualization

Protein structures were retrieved from the AlphaFold Protein Structure Database (<https://alphafold.com/>). Structural clustering was performed using the Foldseek-cluster algorithm [99] with a coverage mode of 0 and a coverage threshold of 0.8. Protein structures were visualized using PyMOL v2.5 with a rainbow color scheme for enhanced clarity.

#### Vector construction and *Agrobacterium*

##### *tumefaciens*-mediated transient expression in *N. benthamiana*

A total of 66 selected CEP genes were amplified from *B. cinerea* cDNA using primers designed to exclude stop codons. The resulting PCR products were cloned into the PVX vector pGR106 [13] using the In-Fusion HD Cloning Kit (Takara).

*Agrobacterium*-mediated transient expression was performed as previously described [152]. Briefly, the PVX vectors were introduced into *A. tumefaciens* strain GV3101 by electroporation. *A. tumefaciens* strains carrying the plasmids were then infiltrated into leaves of 4–5-week-old *N. benthamiana* plants grown at 25°C. To assess the cell death-inducing activity of CEPs, leaves were infiltrated with *A. tumefaciens* carrying the respective CEP-PVX plasmids. To examine the inhibition of cell death induction, leaves were co-infiltrated with *A. tumefaciens* carrying both the CEP-PVX and BAX-PVX plasmids. Observations and photographs were taken 5–7 days after infiltration. All experiments were repeated three times.

#### Abbreviations

CEPs	Candidate effector proteins
CDIPs	Cell death-inducing proteins
PCWDEs	Plant cell wall degrading enzymes
sRNAs	Small RNAs
ETI	Effector-triggered immunity
PTI	PAMP-triggered immunity
PAMPs	Pathogen-associated molecular patterns
hpi	Hour post-infection
PCA	Principal component analysis
FPKM	Fragments per kilobase of transcript per million mapped reads
DEG	Differentially expressed gene
GO	Gene Ontology
KEGG	Kyoto Encyclopedia of Genes and Genomes
ROS	Reactive oxygen species
CAZyme	Carbohydrate-active enzyme
MAX	Magnaporthe Avr and ToxB-like

## Supplementary Information

The online version contains supplementary material available at <https://doi.org/10.1186/s12915-024-02043-4>.

Additional file 1: Fig. S1. Calibration of dual RNA-seq data using qRT-PCR. A Comparison of expression patterns for *A. thaliana* defense-related genes (*AtPR1*, *AtRBOHD*, *AtPDF1.2*, *AtWRKY18*) as determined by qRT-PCR and RNA-seq. Data represent means of three biological replicates with error bars indicating standard deviation. B Comparison of expression patterns for *B. cinerea* pathogenicity-related genes (*BcCrh1*, *BcHip1*, *BcXYG1*, *BcIEB1*) as determined by qRT-PCR and RNA-seq. Data represent means of three biological replicates with error bars indicating standard deviation. Fig. S2. Assessment of the RNA-Seq data set of *A. thaliana* during *B. cinerea* infection. A Distribution of FPKM values for *A. thaliana* transcripts. B Correlation heatmap illustrating the relationships between gene expression profiles across different time points of *B. cinerea* infection in *A. thaliana*. C PCA of RNA-seq data, visualizing the overall variance and relationships between samples based on their gene expression patterns. Fig. S3. Assessment of the RNA-Seq data set of *B. cinerea* during infection. A Correlation heatmap of *B. cinerea* transcripts revealing four distinct transcriptional stages. B Distribution of FPKM values for *B. cinerea* transcripts. Fig. S4. Cluster size and the soft power analysis for Mfuzz. (Supports Figs. 3 and 4). A-B Optimal number of clusters determined by the Elbow method using Mfuzz in *B. cinerea* (A) and *A. thaliana* (B). The Elbow method identifies the optimal number of clusters by finding the point at which adding more clusters does not significantly improve the within-cluster sum of squares. C-D Soft power analysis to obtain the optimized power number in *B. cinerea* (C) and *A. thaliana* (D). The cut-off threshold indicated that the total RNA-Seq data set from infected rice samples could be divided into 9 and 8 co-expression modules, respectively. Fig. S5. KEGG pathway enrichment analysis of each co-expression module in *B. cinerea* (A) and *A. thaliana* (B). Bubble plots display the top enriched pathways for each module ( $p$ -value  $< 0.05$ ). Fig. S6. Expression dynamics of genes involved in *A. thaliana* disease resistance pathways. Heatmap illustrating the expression patterns of genes associated with various disease resistance pathways in *A. thaliana*, including salicylic acid (SA), jasmonic acid (JA), ethylene (ET), reactive oxygen species (ROS), callose deposition, calmodulin signaling, phytoalexin biosynthesis, mitogen-activated protein kinase (MAPK) cascades, MYB transcription factors, WRKY transcription factors, and ethylene response factors (ERF). Fig. S7. Functional annotation of CEPs using HMMER and dbCAN3. A Distribution of CEPs annotation based on predicted functions. CEPs were categorized as CAZymes, Peptidase, Lipase, and others. B Proportion of CAZyme-encoding genes within each temporal expression module. C Comparison of CEPs subcellular localization predictions using WoLF PSORT, LOCALIZER, and BUSCA tools. The Venn diagram displays the predicted localization of CEPs to apoplast, cytoplasm, and nucleus. Fig. S8. Distribution of 591 *B. cinerea* CEP genes loci on chromosomes. (Supports Fig. 5B). Genetic map showing the order and relative distribution of CEP loci among the 18 chromosomes of *B. cinerea*. The positions were determined by analysis against the B05.10 reference genome. Fig. S9. Number of CEPs in each 3D structure cluster. Fig. S10. Structural alignment of *BcCDI1* and *BcIEB1*. The method used for sequence alignment is TM-align.

Additional file 2: Table S1. Summary of read counts and mapping statistics for *B. cinerea* transcriptome analysis.

Additional file 3: Table S2. Summary of read counts and mapping statistics for *A. thaliana* transcriptome analysis.

Additional file 4: Table S3. DEGs in *B. cinerea* at each time point.

Additional file 5: Table S4. *B. cinerea* genes in co-expression modules during infection.

Additional file 6: Table S5. *A. thaliana* genes in co-expression modules during *B. cinerea* infection.

Additional file 7: Table S6. Prediction of effector proteins among BSPs using EffectorP and DeepRedEff.

Additional file 8: Table S7. Annotation of *B. cinerea* CEPs using HMMER and dbCAN3.

Additional file 9: Table S8. Subcellular localization prediction of CEPs using WoLF PSORT, LOCALIZER, and BUSCA Tools.

Additional file 10: Table S9. Information of the 25 species and clustering statistics.

Additional file 11: Table S10. List of orthologous genes across 25 species.

Additional file 12: Table S11. List of paralogous genes in *B. cinerea* CEPs.

Additional file 13: Table S12. Expression modules and structure clusters of *B. cinerea* CEPs.

Additional file 14: Table S13. Information on tested CEPs.

Additional file 15: Table S14. Primers used in this study.

Additional file 16: 3D structure of CEPs.

## Acknowledgements

The authors thank Prof. Tao Chen from the College of Plant Science and Technology, Huazhong Agricultural University, for kindly providing the vectors PVX and PbE3-2-PVX. We are also grateful to Prof. Weidong Chen from the USDA Agricultural Research Service for critical reading and constructive suggestions on the manuscript.

## Authors' contributions

JFW and LY conceived and designed the project. JFW and QZ performed experimental work. JFW performed bioinformatic analysis. JFW wrote the manuscript. LY, GQL, MDW and JZ revised the manuscript. All authors read and approved the final manuscript.

## Funding

This research was funded by the Fundamental Research Funds for the Central Universities 2662020ZKPY010 (LY) and Foundation of Guangdong Provincial Key Laboratory of High Technology for Plant Protection (Zhizhong 2023-03) (J.Z.).

## Data availability

The data that support the findings of this study have been deposited into SRA of the NCBI repository with accession number PRJNA1158549.

## Declarations

### Ethics approval and consent to participate

Not applicable.

### Consent for publication

Not applicable.

### Competing interests

The authors declare no competing interests.

Received: 1 June 2024 Accepted: 14 October 2024

Published online: 21 October 2024

## References

- Dean R, Van Kan JAL, Pretorius ZA, Hammond-Kosack KE, Di Pietro A, Spanu PD, et al. The top 10 fungal pathogens in molecular plant pathology. *Mol Plant Pathol*. 2012;13(4):414–30.
- Schumacher J. Signal transduction cascades regulating differentiation and virulence in *Botrytis cinerea*. In: *Botryotis the fungus, the pathogen and its management in agricultural systems*. Switzerland: Springer International Publishing; 2016. p 247–67.
- Williamson B, Tudzynski B, Tudzynski P, Van Kan JAL. *Botrytis cinerea*: the cause of grey mould disease. *Mol Plant Pathol*. 2007;8(5):561–80.
- Bi K, Liang Y, Mengiste T, Sharon A. Killing softly: a roadmap of *Botrytis cinerea* pathogenicity. *Trends Plant Sci*. 2023;28(2):211–22.

5. Mengiste T. Plant immunity to necrotrophs. *Annu Rev Phytopathol.* 2012;50:267–94.
6. Cheung N, Tian L, Liu X, Li X. The destructive fungal pathogen *Botrytis cinerea*-Insights from genes studied with mutant analysis. *Pathogens.* 2020;9(11):923.
7. Urban M, Cuzick A, Seager J, Wood V, Rutherford K, Venkatesh SY, et al. PHL-base: the pathogen-host interactions database. *Nucleic Acids Res.* 2020;48(D1):D613–20.
8. Shlezinger N, Minz A, Gur Y, Hatam I, Dagdas YF, Talbot NJ, et al. Anti-apoptotic machinery protects the necrotrophic fungus *Botrytis cinerea* from host-induced apoptotic-like cell death during plant infection. *PLoS Pathog.* 2011;7(8):e1002185.
9. Veloso J, van Kan JAL. Many Shades of Grey in *Botrytis*-host plant interactions. *Trends Plant Sci.* 2018;23(7):613–22.
10. Liao CJ, Hailemariam S, Sharon A, Mengiste T. Pathogenic strategies and immune mechanisms to necrotrophs: differences and similarities to biotrophs and hemibiotrophs. *Curr Opin Plant Biol.* 2022;69:102291.
11. ten Have A, Mulder W, Visser J, van Kan JA. The endopolygalacturonase gene *Bcpg1* is required for full virulence of *Botrytis cinerea*. *Mol Plant-Microbe Interact.* 1998;11(10):1009–16.
12. Ji D, Liu W, Cui X, Liu K, Liu Y, Huang X, et al. A receptor-like kinase SIFERL mediates immune responses of tomato to *Botrytis cinerea* by recognizing BcPG1 and fine-tuning MAPK signaling. *New Phytol.* 2023;240(3):1189–201.
13. Ma Z, Song T, Zhu L, Ye W, Wang Y, Shao Y, et al. A Phytophthora sojae glycoside hydrolase 12 protein is a major virulence factor during soybean infection and is recognized as a PAMP. *Plant Cell.* 2015;27(7):2057–72.
14. Kou Y, Shi H, Qiu J, Tao Z, Wang W. Effectors and environment modulating rice blast disease: from understanding to effective control. *Trends Microbiol.* 2024;S0966-842X(24)00072-6.
15. Kabbage M, Yarden O, Dickman MB. Pathogenic attributes of *Sclerotinia sclerotiorum*: switching from a biotrophic to necrotrophic lifestyle. *J Exp Plant Biol.* 2015;233:53–60.
16. Weiberg A, Wang M, Lin FM, Zhao H, Zhang Z, Kaloshian I, et al. Fungal small RNAs suppress plant immunity by hijacking host RNA interference pathways. *Science.* 2013;342(6154):118–23.
17. Yan X, Tang B, Ryder LS, MacLean D, Were VM, Eseola AB, et al. The transcriptional landscape of plant infection by the rice blast fungus *Magnaporthe oryzae* reveals distinct families of temporally co-regulated and structurally conserved effectors. *Plant Cell.* 2023;35(5):1360–85.
18. Lanver D, Müller AN, Happel P, Schweizer G, Haas FB, Franitz M, et al. The biotrophic development of *Ustilago maydis* studied by RNA-Seq analysis. *Plant Cell.* 2018;30(2):300–23.
19. Gay EJ, Soyer JL, Lapalu N, Linglin J, Fudal I, Da Silva C, et al. Large-scale transcriptomics to dissect 2 years of the life of a fungal phytopathogen interacting with its host plant. *BMC Biol.* 2021;19(1):55.
20. Evangelisti E, Gogleva A, Hainaux T, Doumane M, Tulin F, Quan C, et al. Time-resolved dual transcriptomics reveal early induced *Nicotiana benthamiana* root genes and conserved infection-promoting *Phytophthora palmivora* effectors. *BMC Biol.* 2017;15(1):39.
21. Bai Y, Wang H, Zhu K, Cheng ZM. The dynamic arms race during the early invasion of woodland strawberry by *Botrytis cinerea* revealed by dual dense high-resolution RNA-seq analyses. *Hortic Res.* 2023;10(12):225.
22. Seong K, Krasileva KV. Prediction of effector protein structures from fungal phytopathogens enables evolutionary analyses. *Nat Microbiol.* 2023;8(1):174–87.
23. Seong K, Krasileva KV. Computational structural genomics unravels common folds and novel families in the secretome of fungal phytopathogen *Magnaporthe oryzae*. *Mol Plant-Microbe Interactions.* 2021;34(11):1267–80.
24. Rocafort M, Bowen JK, Hassing B, Cox MP, McGreal B, De La Rosa S, et al. The *Venturia inaequalis* effector repertoire is dominated by expanded families with predicted structural similarity, but unrelated sequence, to avirulence proteins from other plant-pathogenic fungi. *BMC Biol.* 2022;20(1):246.
25. Staats M, van Kan JAL. Genome update of *Botrytis cinerea* strains B05.10 and T4. *Eukaryot Cell.* 2012;11(11):1413–4.
26. Cheng CY, Krishnakumar V, Chan AP, Thibaud-Nissen F, Schobel S, Town CD. Araport11: a complete reannotation of the *Arabidopsis thaliana* reference genome. *Plant J.* 2017;89(4):789–804.
27. Kumar L, Futschik ME. Mfuzz: a software package for soft clustering of microarray data. *Bioinformatics.* 2007;2(1):5–7.
28. Yan L, Yang Q, Sundin GW, Li H, Ma Z. The mitogen-activated protein kinase kinase BOSS is involved in regulating vegetative differentiation and virulence in *Botrytis cinerea*. *Fungal Genet Biol.* 2010;47(9):753–60.
29. Ren W, Liu N, Yang Y, Yang Q, Chen C, Gao Q. The sensor proteins BcSho1 and BcSln1 are involved in, though not essential to, vegetative differentiation, pathogenicity and osmotic stress tolerance in *Botrytis cinerea*. *Front Microbiol.* 2019;10:328.
30. Yang Q, Yin D, Yin Y, Cao Y, Ma Z. The response regulator BcSkn7 is required for vegetative differentiation and adaptation to oxidative and osmotic stresses in *Botrytis cinerea*. *Mol Plant Pathol.* 2015;16(3):276–87.
31. Müller N, Lerch M, Schumacher J, Zimmer D, Könnel A, Klug K, et al. Investigations on VELVET regulatory mutants confirm the role of host tissue acidification and secretion of proteins in the pathogenesis of *Botrytis cinerea*. *New Phytol.* 2018;219(3):1062–74.
32. Sun J, Sun CH, Chang HW, Yang S, Liu Y, Zhang MZ, et al. Cyclophilin BcCyp2 regulates infection-related development to facilitate virulence of the gray mold fungus *Botrytis cinerea*. *Int J Mol Sci.* 2021;22(4):1694.
33. Dagdas YF, Yoshino K, Dagdas G, Ryder LS, Bielska E, Steinberg G, et al. Septin-mediated plant cell invasion by the rice blast fungus. *Magnaporthe oryzae* Science. 2012;336(6088):1590–5.
34. Yin Y, Wu S, Chui C, Ma T, Jiang H, Hahn M, et al. The MAPK kinase Bcmkk1 suppresses oxalic acid biosynthesis via impeding phosphorylation of BcRim15 by BcSch9 in *Botrytis cinerea*. *PLoS Pathog.* 2018;14(9):e1007285.
35. Rui O, Hahn M. The Slt2-type MAP kinase Bmp3 of *Botrytis cinerea* is required for normal saprotrophic growth, conidiation, plant surface sensing and host tissue colonization. *Mol Plant Pathol.* 2007;8(2):173–84.
36. Zhang Z, Li H, Qin G, He C, Li B, Tian S. The MADS-Box transcription factor Bcmads1 is required for growth, sclerotia production and pathogenicity of *Botrytis cinerea*. *Sci Rep.* 2016;6:33901.
37. An B, Li B, Li H, Zhang Z, Qin G, Tian S. Aquaporin8 regulates cellular development and reactive oxygen species production, a critical component of virulence in *Botrytis cinerea*. *New Phytol.* 2016;209(4):1668–80.
38. Viehues A, Heller J, Temme N, Tudzynski P. Redox systems in *Botrytis cinerea*: impact on development and virulence. *Mol Plant-Microbe Interact.* 2014;27(8):858–74.
39. Siewers V, Viaud M, Jimenez-Teja D, Collado IG, Gronover CS, Pradier JM, et al. Functional analysis of the cytochrome P450 monooxygenase gene bcb01 of *Botrytis cinerea* indicates that botrydial is a strain-specific virulence factor. *Mol Plant-Microbe Interact.* 2005;18(6):602–12.
40. Frías M, González C, Brito N. BcSpl1, a cerato-platinin family protein, contributes to *Botrytis cinerea* virulence and elicits the hypersensitive response in the host. *New Phytol.* 2011;192(2):483–95.
41. Zhu W, Ronen M, Gur Y, Minz-Dub A, Masrati G, Ben-Tal N, et al. BcXYG1, a Secreted xyloglucanase from *Botrytis cinerea*, triggers both cell death and plant immune responses. *Plant Physiol.* 2017;175(1):438–56.
42. Schouten A, Van Baarlen P, Van Kan JAL. Phytoxic Nep1-like proteins from the necrotrophic fungus *Botrytis cinerea* associate with membranes and the nucleus of plant cells. *New Phytol.* 2008;177(2):493–505.
43. Gronover CS, Kasulke D, Tudzynski P, Tudzynski B. The role of G protein alpha subunits in the infection process of the gray mold fungus *Botrytis cinerea*. *Mol Plant-Microbe Interact.* 2001;14(11):1293–302.
44. Schumacher J. DHN melanin biosynthesis in the plant pathogenic fungus *Botrytis cinerea* is based on two developmentally regulated key enzyme (PKS)-encoding genes. *Mol Microbiol.* 2016;99(4):729–48.
45. Schumacher J, Simon A, Cohrs KC, Viaud M, Tudzynski P. The transcription factor BcLTF1 regulates virulence and light responses in the necrotrophic plant pathogen *Botrytis cinerea*. *PLoS Genet.* 2014;10(1):e1004040.
46. Brandhoff B, Simon A, Dornieden A, Schumacher J. Regulation of conidiation in *Botrytis cinerea* involves the light-responsive transcriptional regulators BcLTF3 and BcREG1. *Curr Genet.* 2017;63(5):931–49.

47. Ren W, Zhang Z, Shao W, Yang Y, Zhou M, Chen C. The autophagy-related gene *BcAtG1* is involved in fungal development and pathogenesis in *Botrytis cinerea*. *Mol Plant Pathol.* 2017;18(2):238–48.
48. Ren W, Sang C, Shi D, Song X, Zhou M, Chen C. Ubiquitin-like activating enzymes BcAtg3 and BcAtg7 participate in development and pathogenesis of *Botrytis cinerea*. *Curr Genet.* 2018;64(4):919–30.
49. Liu N, Ren W, Li F, Chen C, Ma Z. Involvement of the cysteine protease BcAtg4 in development and virulence of *Botrytis cinerea*. *Curr Genet.* 2019;65(1):293–300.
50. Ren W, Liu N, Sang C, Shi D, Zhou M, Chen C, et al. The autophagy gene *BcATG8* regulates the vegetative differentiation and pathogenicity of *Botrytis cinerea*. *Appl Environ Microbiol.* 2018;84(11):e02455-17.
51. Narukawa H, Yokoyama R, Kuroha T, Nishitani K. Host-produced ethylene is required for marked cell expansion and endoreduplication in dodder search hyphae. *Plant Physiol.* 2021;185(2):491–502.
52. Hinz M, Wilson IW, Yang J, Buerstenbinder K, Llewellyn D, Dennis ES, et al. Arabidopsis RAP2.2: an ethylene response transcription factor that is important for hypoxia survival. *Plant Physiol.* 2010;153(2):757–72.
53. Johansson ON, Fantozi E, Fahlberg P, Nilsson AK, Buhot N, Tör M, et al. Role of the penetration-resistance genes PEN1, PEN2 and PEN3 in the hypersensitive response and race-specific resistance in *Arabidopsis thaliana*. *Plant J.* 2014;79(3):466–76.
54. Kadota Y, Sklenar J, Derbyshire P, Stransfeld L, Asai S, Ntoukakis V, et al. Direct regulation of the NADPH oxidase RBOHD by the PRR-associated kinase BIK1 during plant immunity. *Mol Cell.* 2014;54(1):43–55.
55. Li Y, Liu K, Tong G, Xi C, Liu J, Zhao H, et al. MPK3/MPK6-mediated phosphorylation of ERF72 positively regulates resistance to *Botrytis cinerea* through directly and indirectly activating the transcription of camalexin biosynthesis enzymes. *J Exp Bot.* 2022;73(1):413–28.
56. Moffat CS, Ingle RA, Wathugala DL, Saunders NJ, Knight H, Knight MR. ERF5 and ERF6 play redundant roles as positive regulators of JA/Et-mediated defense against *Botrytis cinerea* in *Arabidopsis*. *PloS One.* 2012;7(4):e35995.
57. Valenzuela-Riffo F, Zúñiga PE, Morales-Quintana L, Lolas M, Cáceres M, Figueroa CR. Priming of defense systems and upregulation of *MYC2* and *JAZ1* genes after *Botrytis cinerea* inoculation in methyl jasmonate-treated strawberry fruits. *Plants.* 2020;9(4):447.
58. Zeng Y, Zheng Z, Hessler G, Zou K, Leng J, Bautor J, et al. *Arabidopsis* phytoalexin deficient 4 promotes the maturation and nuclear accumulation of immune-related cysteine protease RD19. *J Exp Bot.* 2024;75(5):1530–46.
59. Nafisi M, Goregaoker S, Botanga CJ, Glawischnig E, Olsen CE, Halkier BA, et al. *Arabidopsis* cytochrome P450 monooxygenase 71A13 catalyzes the conversion of indole-3-acetaldoxime in camalexin synthesis. *Plant Cell.* 2007;19(6):2039–52.
60. Liu S, Kracher B, Ziegler J, Birkenbihl RP, Somssich IE. Negative regulation of ABA signaling by WRKY33 is critical for *Arabidopsis* immunity towards *Botrytis cinerea* 2100. *eLife.* 2015;4:e07295.
61. Zhang B, Shao L, Wang J, Zhang Y, Guo X, Peng Y, et al. Phosphorylation of ATG18a by BAK1 suppresses autophagy and attenuates plant resistance against necrotrophic pathogens. *Autophagy.* 2021;17(9):2093–110.
62. El Oirdi M, Bouarab K. Plant signalling components EDS1 and SGT1 enhance disease caused by the necrotrophic pathogen *Botrytis cinerea*. *New Phytol.* 2007;175(1):131–9.
63. Veronese P, Nakagami H, Bluhm B, Abuqamar S, Chen X, Salmeron J, et al. The membrane-anchored botrytis-induced kinase1 plays distinct roles in *Arabidopsis* resistance to necrotrophic and biotrophic pathogens. *Plant Cell.* 2006;18(1):257–73.
64. Thomma BP, Eggemont K, Penninckx IA, Mauch-Mani B, Vogelsang R, Cammue BP, et al. Separate jasmonate-dependent and salicylate-dependent defense-response pathways in *Arabidopsis* are essential for resistance to distinct microbial pathogens. *Proc Natl Acad Sci U S A.* 1998;95(25):15107–11.
65. Stepanova AN, Alonso JM. Ethylene signaling pathway. *Sci STKE.* 2005;2005(276):cm3.
66. Dolgikh VA, Pukhovaya EM, Zemlyanskaya EV. Shaping ethylene response: the role of EIN3/EIL1 transcription factors. *Front Plant Sci.* 2019;10:1030.
67. Jacobs AK, Lipka V, Burton RA, Panstruga R, Strizhov N, Schulze-Lefert P, et al. An *Arabidopsis* Callose Synthase, GSL5, is required for wound and papillary callose formation. *Plant Cell.* 2003;15(11):2503–13.
68. Töller A, Brownfield L, Neu C, Twell D, Schulze-Lefert P. Dual function of *Arabidopsis* glucan synthase-like genes GSL8 and GSL10 in male gametophyte development and plant growth. *Plant J.* 2008;54(5):911–23.
69. Parisy V, Poinsot B, Owianowski L, Buchala A, Glazebrook J, Mauch F. Identification of PAD2 as a gamma-glutamylcysteine synthetase highlights the importance of glutathione in disease resistance of *Arabidopsis*. *Plant J.* 2007;49(1):159–72.
70. Schuhegger R, Nafisi M, Mansourova M, Petersen BL, Olsen CE, Svatos A, et al. CYP71B15 (PAD3) catalyzes the final step in camalexin biosynthesis. *Plant Physiol.* 2006;141(4):1248–54.
71. Knotz C, Ringler J, Dangl JL, Eulgem T. *Arabidopsis* WRKY70 is required for full RPP4-mediated disease resistance and basal defense against Hyaloperonospora parasitica. *Mol Plant-Microbe Interact.* 2007;20(2):120–8.
72. Berrocal-Lobo M, Molina A, Solano R. Constitutive expression of ethylene-response-factor1 in *Arabidopsis* confers resistance to several necrotrophic fungi. *Plant J.* 2002;29(1):23–32.
73. Krogh A, Larsson B, von Heijne G, Sonnhammer EL. Predicting transmembrane protein topology with a hidden Markov model: application to complete genomes. *J Mol Biol.* 2001;305(3):567–80.
74. AlmagroArmenteros JJ, Tsirigos KD, Sønderby CK, Petersen TN, Winther O, Brunak S, et al. SignalP 5.0 improves signal peptide predictions using deep neural networks. *Nat Biotechnol.* 2019;37(4):420–3.
75. Bi K, Scalschi L, Jaiswal N, Mengiste T, Fried R, Sanz AB, et al. The *Botrytis cinerea* Crh1 transglycosylase is a cytoplasmic effector triggering plant cell death and defense response. *Nat Commun.* 2021;12(1):2166.
76. Liang Y, Bi K, Sharon A. The *Botrytis cinerea* transglycosylase BcCrh4 is a cell death-inducing protein with cell death-promoting and -suppressing domains. *Plant Cell Environ.* 2023;47(1):354–71.
77. Nie J, Yin Z, Li Z, Wu Y, Huang L. A small cysteine-rich protein from two kingdoms of microbes is recognized as a novel pathogen-associated molecular pattern. *New Phytol.* 2019;222(2):995–1011.
78. Nie J, Zhou W, Liu J, Tan N, Zhou JM, Huang L. A receptor-like protein from *Nicotiana benthamiana* mediates VmE02 PAMP-triggered immunity. *New Phytol.* 2021;229(4):2260–72.
79. Frías M, González M, González C, Brito N. A 25-residue peptide from *Botrytis cinerea* Xylanase BcXyn11A elicits plant defenses. *Front Plant Sci.* 2019;10:474.
80. Zhu W, Yu M, Xu R, Bi K, Yu S, Xiong C, et al. *Botrytis cinerea* BcSP2 protein is a late infection phase, cytotoxic effector. *Environ Microbiol.* 2022;24(8):3420–35.
81. Potter SC, Luciani A, Eddy SR, Park Y, Lopez R, Finn RD. HMMER web server: 2018 update. *Nucleic Acids Res.* 2018;46(W1):W200–204.
82. Yin Y, Mao X, Yang J, Chen X, Mao F, Xu Y. dbCAN: a web resource for automated carbohydrate-active enzyme annotation. *Nucleic Acids Res.* 2012;40:W445–51.
83. Sperschneider J, Dodds PN. EffectorP 3.0: prediction of apoplastic and cytoplasmic effectors in fungi and oomycetes. *Mol Plant-Microbe Interact.* 2022;35(2):146–56.
84. Kristianingsih R, MacLean D. Accurate plant pathogen effector protein classification ab initio with deeppredef: an ensemble of convolutional neural networks. *BMC Bioinformatics.* 2021;22(1):372.
85. Horton P, Park KJ, Obayashi T, Fujita N, Harada H, Adams-Collier CJ, et al. WoLF PSORT: protein localization predictor. *Nucleic Acids Res.* 2007;35:W585–587.
86. Sperschneider J. LOCALIZER: subcellular localization prediction of both plant and effector proteins in the plant cell. *Sci Rep.* 2017;7:44598.
87. Savojardo C, Martelli PL, Fariselli P, Profitti G, Casadio R. BUSCA: an integrative web server to predict subcellular localization of proteins. *Nucleic Acids Res.* 2018;46:W459–466.
88. Li L, Stoeckert CJ, Roos DS. OrthoMCL: identification of ortholog groups for eukaryotic genomes. *Genome Res.* 2003;13(9):2178–89.
89. Wang Y, Tang H, Debarry JD, Tan X, Li J, Wang X, et al. MCScanX: a toolkit for detection and evolutionary analysis of gene synteny and collinearity. *Nucleic Acids Res.* 2012;40(7):e49.
90. Camacho C, Coulouris G, Avagyan V, Ma N, Papadopoulos J, Bealer K, et al. BLAST+: architecture and applications. *BMC Bioinformatics.* 2009;10:421.
91. Raffaele S, Kamoun S. Genome evolution in filamentous plant pathogens: why bigger can be better. *Nat Rev Microbiol.* 2012;10(6):417–30.
92. Jumper J, Evans R, Pritzel A, Green T, Figurnov M, Ronneberger O, et al. Highly accurate protein structure prediction with AlphaFold. *Nature.* 2021;596(7873):583–9.

93. Lahfa M, Barthe P, De Guillen K, Cesari S, Raji M, Kroj T, et al. The structural landscape and diversity of *Pyricularia oryzae* MAX effectors. *PLoS Pathog.* 2024;20(5):e1012176.
94. Lazar N, Mesarich CH, Petit-Houdenot Y, Talbi N, de la Li Sierra-Gallay I, Zélie E, et al. A new family of structurally conserved fungal effectors displays epistatic interactions with plant resistance proteins. *PLoS Pathog.* 2022;18(7):e1010664.
95. Blondeau K, Blaise F, Graille M, Kale SD, Linglin J, Ollivier B, et al. Crystal structure of the effector AvrLm4-7 of *Leptosphaeria maculans* reveals insights into its translocation into plant cells and recognition by resistance proteins. *Plant J.* 2015;83(4):610–24.
96. Sarma GN, Manning VA, Ciuffetti LM, Karplus PA. Structure of Ptr ToxA: an RGD-containing host-selective toxin from *Pyrenophora tritici-repentis*. *Plant Cell.* 2005;17(11):3190–202.
97. Nyarko A, Singaravel KK, Figueroa M, Manning VA, Pandelova I, Wolpert TJ, et al. Solution NMR structures of *Pyrenophora tritici-repentis* ToxB and its inactive homolog reveal potential determinants of toxin activity. *J Biol Chem.* 2014;289(37):25946–56.
98. Mesarich CH, Ökmen B, Rovenich H, Griffiths SA, Wang C, Karimi Jashni M, et al. Specific hypersensitive response-associated recognition of new apoplastic effectors from *Cladosporium fulvum* in wild tomato. *Mol Plant-Microbe Interact.* 2018;31(1):145–62.
99. van Kempen M, Kim SS, Tumescheit C, Mirdita M, Lee J, Gilchrist CLM, Söding J, Steiniger M. Fast and accurate protein structure search with Foldseek. *Nat Biotechnol.* 2024;42(2):243–6.
100. Li C, Luo S, Feng L, Wang Q, Cheng J, Xie J, et al. Protist ubiquitin ligase effector PbE3-2 targets cysteine protease RD21A to impede plant immunity. *Plant Physiol.* 2024;194(3):1764–78.
101. Marschall R, Tudzynski P. Bclqg1, a fungal IQGAP homolog, interacts with NADPH oxidase, MAP kinase and calcium signaling proteins and regulates virulence and development in *Botrytis cinerea*. *Mol Microbiol.* 2016;101(2):281–98.
102. Chen T, Zhang Z, Chen Y, Li B, Tian S. *Botrytis cinerea*. *Curr Biol.* 2023;33(11):R460–462.
103. Hou J, Feng H, Chang H, Liu Y, Li G, Yang S, et al. The H3K4 demethylase Jar1 orchestrates ROS production and expression of pathogenesis-related genes to facilitate *Botrytis cinerea* virulence. *New Phytol.* 2020;225(2):930–47.
104. Segmüller N, Kokkelink L, Giesbert S, Odinius D, van Kan J, Tudzynski P. NADPH oxidases are involved in differentiation and pathogenicity in *Botrytis cinerea*. *Mol Plant-Microbe Interact.* 2008;21(6):808–19.
105. Li H, Zhang Z, He C, Qin G, Tian S. Comparative proteomics reveals the potential targets of BcNoxR, a putative regulatory subunit of NADPH oxidase of *Botrytis cinerea*. *Mol Plant-Microbe Interact.* 2016;29(12):990–1003.
106. Siegmund U, Marschall R, Tudzynski P. BcNoxD, a putative ER protein, is a new component of the NADPH oxidase complex in *Botrytis cinerea*. *Mol Microbiol.* 2015;95(6):988–1005.
107. Zhang M, Trushina NK, Lang T, Hahn M, Pasmanik-Chor M, Sharon A. Serine peptidases and increased amounts of soluble proteins contribute to heat priming of the plant pathogenic fungus *Botrytis cinerea*. *MBio.* 2023;14(4):e0107723.
108. Choquer M, Rascle C, Gonçalves IR, de Vallée A, Ribot C, Loisel E, et al. The infection cushion of *Botrytis cinerea*: a fungal “weapon” of plant-biomass destruction. *Environ Microbiol.* 2021;23(4):2293–314.
109. Windram O, Madhou P, McHattie S, Hill C, Hickman R, Cooke E, et al. *Arabidopsis* defense against *Botrytis cinerea*: chronology and regulation deciphered by high-resolution temporal transcriptomic analysis. *Plant Cell.* 2012;24(9):3530–57.
110. Wang S, He B, Wu H, Cai Q, Ramírez-Sánchez O, Abreu-Goodger C, et al. Plant mRNAs move into a fungal pathogen via extracellular vesicles to reduce infection. *Cell Host Microbe.* 2024;32(1):93–105.e6.
111. Zhu W, Dong H, Xu R, You J, Yan DZ, Xiong C, et al. *Botrytis cinerea* BcCDI1 protein triggers both plant cell death and immune response. *Front Plant Sci.* 2023;14:1136463.
112. Leisen T, Bietz F, Werner J, Wegner A, Schaffrath U, Scheuring D, et al. CRISPR/Cas with ribonucleoprotein complexes and transiently selected telomere vectors allows highly efficient marker-free and multiple genome editing in *Botrytis cinerea*. *PLoS Pathog.* 2020;16(8):e1008326.
113. Arroyo-Velez N, González-Fuente M, Peeters N, Lauber E, Noël LD. From effectors to effectomes: are functional studies of individual effectors enough to decipher plant pathogen infectious strategies? *PLoS Pathog.* 2020;16(12):e1009059.
114. Morgan W, Kamoun S. RXLR effectors of plant pathogenic oomycetes. *Curr Opin Microbiol.* 2007;10(4):332–8.
115. Valandro F, Menguer PK, Cabreira-Cagliari C, Margis-Pinheiro M, Cagliari A. Programmed cell death (PCD) control in plants: new insights from the *Arabidopsis thaliana* deathosome. *Plant Sci.* 2020;299:110603.
116. Cui F, Li X, Wu W, Luo W, Wu Y, Brosché M, et al. Ectopic expression of botrytis susceptible1 reveals its function as a positive regulator of wound-induced cell death and plant susceptibility to *Botrytis*. *Plant Cell.* 2022;34(10):4105–16.
117. Andrews LB, Curtis WR. Comparison of transient protein expression in tobacco leaves and plant suspension culture. *Biotechnol Prog.* 2005;21(3):946–52.
118. Redkar A, Jaeger E, Doeblemann G. Visualization of growth and morphology of fungal hyphae in planta using WGA-AF488 and propidium iodide co-staining. *Bio Protoc.* 2018;8(14):e2942.
119. Wu T, Hu E, Xu S, Chen M, Guo P, Dai Z, et al. clusterProfiler 4.0: a universal enrichment tool for interpreting omics data. *Innovation.* 2021;2(3):100141.
120. Kolberg L, Raudvere U, Kuzmin I, Adler P, Vilo J, Peterson H. g:Profiler-interoperable web service for functional enrichment analysis and gene identifier mapping. *Nucleic Acids Res.* 2023;51(W1):W207–212.
121. Zhang J. ClusterGVIS: one-step to cluster and visualize gene expression matrix. 2022. <https://github.com/junjunlab/ClusterGVIS>.
122. Valero-Jiménez CA, Steentjes MBF, Slot JC, Shi-Kunne X, Scholten OE, van Kan JAL. Comparative genomics of *Sclerotiniaceae*. 2020. GenBank <https://www.ncbi.nlm.nih.gov/bioproject/PRJNA494516/>.
123. Valero-Jiménez CA, Steentjes MBF, Slot JC, Shi-Kunne X, Scholten OE, van Kan JAL. Dynamics in secondary metabolite gene clusters in otherwise highly syntenic and stable genomes in the fungal genus *botrytis*. *Genome Biol Evol.* 2020;12(12):2491–507.
124. Amselem J, Cuomo CA, van Kan JA, Viald M, Benito EP, Couloux A, et al. Genomic analysis of the necrotrophic fungal pathogens *Sclerotinia sclerotiorum* and *Botrytis cinerea*. *PLoS Genet.* 2011;7(8):e1002230.
125. De Miccolis Angelini RM, Romanazzi G, Pollastro S, Rotolo C, Faretra F, Landi L. *Monilinia fructicola* Mfrc123, genome sequencing and assembly. 2019. GeneBank [https://www.ncbi.nlm.nih.gov/datasets/genome/GCA\\_008692225.1/](https://www.ncbi.nlm.nih.gov/datasets/genome/GCA_008692225.1/).
126. Hane JK, Lowe RG, Solomon PS, Tan KC, Schoch CL, Spatafora JW, et al. *Parastagonospora nodorum* SN15, genome sequencing and assembly. 2017. GeneBank [https://www.ncbi.nlm.nih.gov/datasets/genome/GCF\\_000146915.1/](https://www.ncbi.nlm.nih.gov/datasets/genome/GCF_000146915.1/).
127. Sharma R, Xia X, Cano LM, Evangelisti E, Kemen E, Judelson H, et al. *Plasmopara halstedii*, genome sequencing and assembly. 2015. GenkBank [https://www.ncbi.nlm.nih.gov/datasets/genome/GCF\\_900000015.1/](https://www.ncbi.nlm.nih.gov/datasets/genome/GCF_900000015.1/).
128. Huang K, Tang J, Zou Y, Sun X, Lan J, Wang W, et al. *Alternaria alternata* SRC1IrK2f, genome sequencing and assembly. 2021. GenkBank [https://www.ncbi.nlm.nih.gov/datasets/genome/GCF\\_001642055.1/](https://www.ncbi.nlm.nih.gov/datasets/genome/GCF_001642055.1/).
129. Yu C, Diao Y, Lu Q, Zhao J, Cui S, Xiong X, et al. *Diplodia corticola* CBS112549, genome sequencing and assembly. 2021. GenkBank [https://www.ncbi.nlm.nih.gov/datasets/genome/GCA\\_023087385.1/](https://www.ncbi.nlm.nih.gov/datasets/genome/GCA_023087385.1/).
130. Li D. *Valsa mali* Vm263, genome sequencing and assembly. 2021. GenkBank [https://www.ncbi.nlm.nih.gov/datasets/genome/GCA\\_02542655.1/](https://www.ncbi.nlm.nih.gov/datasets/genome/GCA_02542655.1/).
131. Mendes-Pereira E, Balesdent MH, Brun H, Rouxel T. *Leptosphaeria maculans* NZT4, genome sequencing and assembly. 2018. GenkBank [https://www.ncbi.nlm.nih.gov/datasets/genome/GCA\\_900465115.1/](https://www.ncbi.nlm.nih.gov/datasets/genome/GCA_900465115.1/).
132. Duplessis S, Cuomo CA, Lin YC, Aerts A, Tisserant E, Veneault-Fourrey C, et al. *Melampsora larici-populina* 98AG31, genome sequencing and assembly. 2011. GenkBank [https://www.ncbi.nlm.nih.gov/datasets/genome/GCF\\_000204055.1/](https://www.ncbi.nlm.nih.gov/datasets/genome/GCF_000204055.1/).
133. Duplessis S, Cuomo CA, Lin YC, Aerts A, Tisserant E, Veneault-Fourrey C, et al. Obligate biotrophy features unraveled by the genomic analysis of rust fungi. *Proc Natl Acad Sci U S A.* 2011;108(22):9166–71.
134. de Jonge R, Bolton MD, Kombrink A, van den Berg GC, Yadeta KA, Thomma BP. *Verticillium dahliae* VdLs.17, genome sequencing and

- assembly. 2011. GenkBank [https://www.ncbi.nlm.nih.gov/datasets/genome/GCF\\_000150675.1/](https://www.ncbi.nlm.nih.gov/datasets/genome/GCF_000150675.1/).
136. Kämper J, Kahmann R, Böker M, Ma LJ, Brefort T, Saville BJ, et al. *Ustilago maydis* 521, genome sequencing and assembly. 2015. GenkBank [https://www.ncbi.nlm.nih.gov/datasets/genome/GCF\\_000328475.2/](https://www.ncbi.nlm.nih.gov/datasets/genome/GCF_000328475.2/).
137. Duplessis S, Cuomo CA, Lin YC, Aerts A, Tisserant E, Veneault-Fourrey C, et al. *Puccinia graminis* sp. *tritici* CRL 75-36-700-3, genome sequencing and assembly. 2008. GenkBank [https://www.ncbi.nlm.nih.gov/datasets/genome/GCF\\_000149925.1/](https://www.ncbi.nlm.nih.gov/datasets/genome/GCF_000149925.1/).
138. Vaghefi N, Kusch S, Németh MZ, Seress D, Braun U, Takamatsu S, et al. *Blumeria graminis* DH14, genome sequencing and assembly. 2021. GenkBank [https://www.ncbi.nlm.nih.gov/datasets/genome/GCA\\_905067625.1/](https://www.ncbi.nlm.nih.gov/datasets/genome/GCA_905067625.1/).
139. Vaghefi N, Kusch S, Németh MZ, Seress D, Braun U, Takamatsu S, et al. Beyond nuclear ribosomal DNA sequences: evolution, taxonomy, and closest known saprobic relatives of powdery mildew fungi (Erysiphaceae) inferred from their first comprehensive genome-scale phylogenetic analyses. *Front Microbiol.* 2022;13:903024.
140. Dean RA, Talbot NJ, Ebbot DJ, Farman ML, Mitchell TK, Orbach MJ, et al. *Pyricularia oryzae* 70-15, genome sequencing and assembly. 2011. GenkBank [https://www.ncbi.nlm.nih.gov/datasets/genome/GCF\\_000002495.2/](https://www.ncbi.nlm.nih.gov/datasets/genome/GCF_000002495.2/).
141. Dean RA, Talbot NJ, Ebbot DJ, Farman ML, Mitchell TK, Orbach MJ, et al. The genome sequence of the rice blast fungus *Magnaporthe grisea*. *Nature.* 2005;434(7036):980–6.
142. Cuomo CA, Güldener U, Xu JR, Trail F, Turgeon BG, Di Pietro A, et al. *Fusarium graminearum* PH-1, genome sequencing and assembly. 2008. GenkBank [https://www.ncbi.nlm.nih.gov/datasets/genome/GCF\\_000240135.3/](https://www.ncbi.nlm.nih.gov/datasets/genome/GCF_000240135.3/).
143. Cuomo CA, Güldener U, Xu JR, Trail F, Turgeon BG, Di Pietro A, et al. The *Fusarium graminearum* genome reveals a link between localized polymorphism and pathogen specialization. *Science.* 2007;317(5843):1400–2.
144. Javed MA, Mukhopadhyay S, Normandeau E, Brochu AS, Pérez-López E. *Plasmidiophora brassicae* Pb3A, genome sequencing and assembly. 2024. GenkBank [https://www.ncbi.nlm.nih.gov/datasets/genome/GCA\\_036867785.1/](https://www.ncbi.nlm.nih.gov/datasets/genome/GCA_036867785.1/).
145. Javed MA, Mukhopadhyay S, Normandeau E, Brochu AS, Pérez-López E. Telomere-to-telomere genome assembly of the clubroot pathogen *Plasmidiophora Brassicae*. *Genome Biol Evol.* 2024;16(6):eve122.
146. Yang D, Luo T, Wei J, Cao C, Li G, Yang L. *Sclerotinia minor* LC41, genome sequencing and assembly. 2021. CNSA <https://db.cngb.org/search/project/CNP0001962/>.
147. Yang D, Luo T, Wei J, Cao C, Li G, Yang L. High-quality genome resource of the phytopathogenic fungus *Sclerotinia minor* LC41, the Causal Agent of Sclerotinia Blight on Lettuce in China. *Plant Dis.* 2022;106(3):1042–4.
148. Hane JK, Lowe RG, Solomon PS, Tan KC, Schoch CL, Spatafora JW, et al. *Parastagonospora nodorum* SN15, genome sequencing and assembly. 2007. GenkBank [https://www.ncbi.nlm.nih.gov/datasets/genome/GCF\\_000146915.1/](https://www.ncbi.nlm.nih.gov/datasets/genome/GCF_000146915.1/).
149. Hane JK, Lowe RG, Solomon PS, Tan KC, Schoch CL, Spatafora JW, et al. Dothideomycete plant interactions illuminated by genome sequencing and EST analysis of the wheat pathogen *Stagonospora nodorum*. *Plant Cell.* 2007;19(11):3347–68.
150. Sun J, Lu F, Luo Y, Bie L, Xu L, Wang Y. OrthoVenn3: an integrated platform for exploring and visualizing orthologous data across genomes. *Nucleic Acids Res.* 2023;51(W1):W397–403.
151. Chen C, Wu Y, Li J, Wang X, Zeng Z, Xu J, et al. TBtools-II: a “one for all, all for one” bioinformatics platform for biological big-data mining. *Mol Plant.* 2023;16(11):1733–42.
152. Wang Q, Han C, Ferreira AO, Yu X, Ye W, Tripathy S, et al. Transcriptional programming and functional interactions within the *Phytophthora sojae* RXLR effector repertoire. *Plant Cell.* 2011;23(6):2064–86.

## Publisher's Note

Springer Nature remains neutral with regard to jurisdictional claims in published maps and institutional affiliations.